FABRICATION AND CHARACTERISATION OF INTERCONNECTS SUITABLE FOR HIGH FREQUENCY ULTRASONIC ARRAY TRANSDUCERS

By Ran Xiao

[redacted]

MRes Science and Engineering of Materials

Supervisor: Prof. Tim Button

24/09/2012

Content

1. Introduction 1

2. Literature Review 3

2.1. ACF Interconnection 3

2.2. Bonding Process of ACF 4

2.3. Requirement of the ACF Interconnection 5

2.4. Characterization for ACF 6

2.5. Different Types of ACFs 12

2.6. Objectives 15

3. Experimental ..... 错误！未定义书签。

3.1. Materials Selection 16

3.2. Experimental Procedure 17

3.2.1. Epoxy Resin Film Tape Casting and Observation of Surface Morphology 17

3.2.2. Preparation of the ACF 19

3.2.3. Measurement of Electric Resistance 23

3.2.4. Reliability Test 24

3.2.5. Microstructure and Morphology Observation 24

3.3. Errors 25

4. Results and Discussion 25

4.1. Effect of Bonding Temperature on Curing Process of the EPOFIX 25

4.2. Effect of Pressure on Curing Process 29

4.3. Effect of Pressure on Electrical Resistance 34

4.4. Effect of Particle Concentration on Electrical Resistance 41

4.5. Effect of Service Time on Electrical Resistance 44

4.6. **Analysis of Defects** 47

5. Conclusions 48

6. Future Work 49

7. References 50

List of Figures

Figure 1: A schematic description of 1-3 composite. The piezoelectric pillars are surrounded by epoxy resin matrix (Bernassau 2010).....1

Figure 2: Schematic diagram of high frequency ultrasonic transducers (Bernassau 2010) 3

Figure 3: Cross section of ACF, the conductive particles is doped in the isolative epoxy resin. (Terasaka et al 1998).....4

Figure 4: Sketch of the ACF interconnection. Conductive particles and plastic particles (plated metal) were compressed by the electrodes. (Terasaka et al 1998) 5

Figure 5: Schematic deformation of a half conductive particle when a contact load is applied. (Woon-Seong Kwon, 2006) 7

Figure 6: (a) Effect of bonding pressure on electrical resistance of ACF (b) Effect of particle concentration on electrical resistance of ACF. (Jong-Woong Kim.2006).....9

Figure 7: Cross-section view of ACF joints (Joog-woong Kim 2006).....10

Figure 8： Optical morphology of deformed conductive particles. The crack of the conductive particle's coating layer could be observed in the pictures. Samples with same particle concentration, bonded at 180℃, hold 20 seconds. (a) applied pressure is 100MPa, (b) applied pressure is 200 MPa (Woon-Seong Kwon.2006) 10

Figure 9: The contact resistance varied with the test time for ACF and standard deviation of ACF using bare aluminum pads at 85℃/85% RH (Al-1, for 1μm aluminum pads; Al-3, for 3μm aluminum pads; Al-5, for 5μm aluminum pads).....11

Figure 10: Cross section of ACF. (1 and 3 - the device, 2 - the ACF, 4 and 5 - electrodes, 6 - conductive particles, 30 - the thermal set polymer, L - the thickness between the electrode, P1 and P2 - the pitch width). (Yamamoto et al 2010) 12

Figure 11: ACF from Maeda et al. (1 - the ACF, 2 - isolative polyamide film, 3 - the conductive silicone resin or conductive particles) (Maeda et al 1997) 13

Figure 12: The manufacturing steps of the ACF which is shown in Figure 11.(1- resist, 2 - the copper foil, 3- polyamide film, 4 - the gold plate, 5 - the through-hole, 6 - silicone resin). (Maeda et al1997) 14

Figure 13: Cross sectional view of a semiconductor device being electrical connected with a substrate via anisotropic conductive film. (4 - conductive polymer bars with 5μm diameter, 8 - ACF, 9 - electrodes, 13 and 10 - device with 10μm minimum pitch size). (Maeda et al1997) 15

Figure 14: The particle distribution of silver coated copper powder 17

Figure 15: Laser particle size analyzer (SYMPATEC Ltd.) 17

Figure 16: Schematic diagram of tape casting. 18

Figure 17: Schematic diagram of sample assembling. (a) Sample without pressure (b) Sample with pressure. 19

Figure 18: The schematic substrate preparation route 20

Figure 19: Gold sputtering (EMITECH Ltd. K575X) 21

Figure 20: Schematic diagram of substrates and ACF assembling 22

Figure 21: Schematic diagram of test circuit of electrical resistivity measurement of ACF 23

Figure 22: Electrode pattern of experiment 24

Figure 23: The relationship between the bonding time and temperature of samples 26

Figure 24: The surface morphology of the samples cured at different temperatures without glass slides cover. The red circles denote impurities and dirt, and the blue circles denote the

air bubbles in the photos; the white spot is the reflection of light-spot. 27

Figure 25: The relationship between the cured time and temperature of the curing state and air bubble appearance states. The samples without the glass slide cover 28

Figure 26: The state of samples varies with curing temperature and time. The samples were covered by glass slide (pressure is 50MPa).....30

Figure 27: The surface morphology of the sample with glass slides cover without pressure at different cured temperatures; the white spot is the reflection of light-spot. 31

Figure 28: The surface morphology of the sample cured at different temperatures with glass slide cover under pressure of 50MPa, the white spot is the reflection of light-spot.....32

Figure 29: The relationship between the time and temperature of the curing state and air bubble appearance states, all samples covered by glass slide.....33

Figure 30: The relationship between the electrical resistance and pressure applied on the ACF, the data points were taken from the average electrical resistance under different pressure, and the curve is trend line.....35

Figure 31: The relationship between horizontal electrical resistance and pressure applied on the surface of ACF. 35

Figure 32: The cross-section of ACF joints bonded under pressure of 0.5MPa, the agglomerated conductive powder is labeled.....36

Figure 33: The cross-section view of ACF joints bonded under 1.5MPa, the agglomerated conductive powder is labeled.....37

Figure 34: Cross-section view of ACF joints bonded under 4.5MPa, the broken agglomerated conductive powder is labeled.....38

Figure 35: Cross-section view of ACF joints bonded under 6MPa, the large single conductive

powder is labeled. 39

Figure 36: Cross-section view of ACF joints bonded under 7.5MPa, the large single conductive powder is labeled. 40

Figure 37: Electrical resistivity of ACF varies as pressure, the data points are calculate from the result of Figure 28 and SEM. 41

Figure 38: Electrical resistance of ACF varies as particle concentration, ACF bonded under condition of 120℃/20min/1.5MPa). 42

Figure 39: Relationship between electric resistance and particle density of ACF calculated from equation 7. 44

Figure 40: Electrical resistance of ACF vary as working time under condition of 80℃/80% RH. Samples were prepared under bonding conditions of 120℃/1.5MPa/20mins; the powder concentration was 3500 particles/mm^2. 45

Figure 41: Cross-section of ACF joint, after 500 hours ageing test, the thickness of ACF is increased. 46

Figure 42: Schematic deformation of a half conductive particle during a long working time. 46

Figure 43; The morphology of conductive powders in ACF joints, where (a) is the area with defect, (b) is the area with no defect, (c) shows the agglomerate of conductive powder. 47

Acknowledgements

I would like to thank my supervisor, Prof. Tim Button, for his guidance, support and confidence in me.

I would like to thank my colleague Yun Jiang and Carl Meggs, Yun Jiang gives me lots of help on the electrode preparing process. Carl Meggs advice and suggestions allow me understand and improve my experiments and project.

I would also like to thank my father Prof. Jianzhong Xiao who has been give me great help for my thesis writing skills and knowledge in characterizing methods.

I would like to thank the University of Birmingham, where I have started my MRes degree.

Abstract

Anisotropic conductive films (ACFs) are widely used in interconnection technologies because they enable ultrafine pitch capability. The high frequency array type device could increase the spatial resolution of the ultrasonic imaging. However the ACF is one of the key materials to realize the fine-scale pitch interconnection in the array type devices. The electrical properties of the ACF and its behavior during the synthesis process are important for the performance improvement. In this thesis the ACF with different conductive particle concentration have been synthesed from silver coated conductive particles and epoxy resin. The electrical properties and microstructures of the ACF have been characterized. The author tries to analysis the influence parameters of processing route on the electrical resistance of the ACF and to improve its performance.

The ACFs are prepared directly from EPOFIX resin and silver coated copper powders with different contents. The minimum electric resistivity in the direction of applied pressure (vertical direction) of 50MPa ρ = 1.00(±0.5)Ωm was achieved, and the value in horizontal direction was 10^6 times larger than in vertical direction, when the mass ratio of EPOFIX resin and silver coated conductive powders is 81:19; the bonding condition is 120℃/20min/1.5MPa. The estimated service life is more than 5 years.

There are four main factors affecting the properties of the ACF: bonding temperature, bonding time, bonding pressure and particle concentration. The bonding temperature is the most important parameter to accelerate the curing/bonding process of the ACF, but heating of the ACF to temperature above 180℃ will induce bubbles in the ACF, because the air does not have enough time to escape from the ACF before it is fully cured. The higher the bonding temperature, the shorter the bonding time.

The electrical resistance in the direction of applied pressure of the ACF varied

with applied pressure and there are three stages. The first stage is the resistance decrease stage when the pressure is at low; this stage is related to contact improvement between the electrode and the conductive particles in the ACF. The second stage is the wide resistance plateau stage when the pressure changes from 2.5MPa to 6MPa. This stage is related to agglomerated particles crashed in ACF. The third stage is the plastic deformation of the conductive particles in ACF, which causes the electrical resistance to increase.

1. Introduction

For many years, ultrasonic imaging has become an important technique applied in medical diagnosis (Frost & Sullivan 2008). Compared to other imaging techniques such as X-ray or computed tomography (CT), ultrasonic imaging can provide a real-time image, like imaging of breathing and pregnancy. Ultrasonic device units are more portable than other imaging device and the main advantage of ultrasonic imaging is the low risk to health compared to X-ray and computed tomography (Natori 2004). The main concern of ultrasonic imaging is the intensity of the ultrasonic beam which may cause tissue heating or mechanical effects (Maulik 2005). However the resolution of ultrasonic imaging is poor compared to other imaging techniques.

In order to improve the resolution, besides increasing the frequency of the ultrasonic transducer, applying the fine scale array type device is needed. This type of transducers could potentially allow a better resolution (Smith and Auld 1991). The array type device is mainly based on the piezoelectric ceramic and epoxy adhesive composites. It could provide a better performance than the single-element transducer (Smith and Auld 1991). A schematic diagram of piezocomposite transducer element is shown in Figure 1.

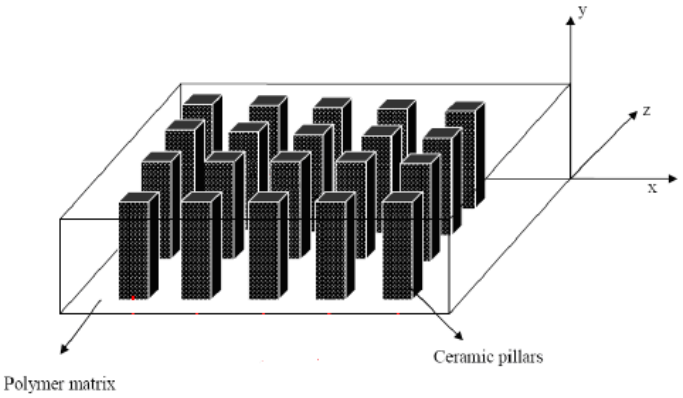

Figure 1: A schematic diagram of 1-3 composite. The piezoelectric pillars are surrounded by epoxy resin matrix (*Bernassau 2010*)

The epoxy resin matrix can absorb the horizontal vibrations which are generated by piezoelectric ceramics and the composite only generates vibration vertically, thus giving a higher receiving sensitivity and larger transmission response. The 1-3 composite structure can also be formed into a complex curved shape that can focus the ultrasound waves to get better resolutions. The performance of array type ultrasonic devices is dependent on the materials involved as well as the geometry and arrangement of the piezoelectric pillars (Smith, Shaulov et al. 1985; Hayward and Hossack 1990).

In an array type device, as we known, the more elements in each array，the better resolution can be achieved (Bernassau 2010). This requires fine scale piezoelectric composites (array elements, pillar diameter is 10-20 μm, for a frequency of 30MHz). There are many limitations of those fine scale composites; one of these limitations is the interconnection. Recently, two types of interconnection technology have been applied: wire bonding and wire free bonding, the latter is most commonly used especially in array type devices, since it can provide a finer scale interconnection rather than wire bonding (wire bonding is limited by the scale of wire). The ACFs (anisotropic conductive film) is the key material in the wire free bonding technology (J.H. Zhang 2003). Many research works have been done on the ACFs. These works mainly focused on the relationship between the performance and the composition of the ACFs, and different ACFs have been developed, but detailed references could not be found especially dealing with the manufacturing process. The aim of the work reported in this thesis is to find a suitable ACF for the fine scale interconnections directly from the widely used epoxy resin and metal particles, and to study the relationship between the performance and the preparation process.

2. Literature Review

2.1. ACF Interconnection

The high frequency ultrasonic transducer is widely used in many fields such as medical applications. An ultrasonic transducer is made of piezoelectric ceramic layers, front matching layer, backing layers, and bonded electrodes. Between these layers, the interconnection is required (Bernassau 2010).

There are two types of interconnection for ultrasonic transducers. One is wire bonding, in which the elements are bonded by very thin conductive wires. The other one is called the wire free bonding. In that regard, the elements are not connected by a conductive wire, but by anisotropic conductive films (ACF). These two types of interconnect are shown in Figure 2.

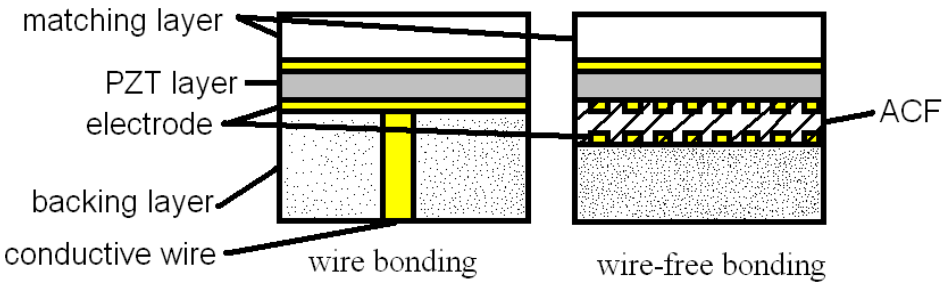

Figure 2: Schematic diagram of high frequency ultrasonic transducers (Bernassau 2010)

The anisotropic conductive films (ACFs) are made of adhesive resin and conducting particles as shown in Figure 3. ACFs are widely used in packaging technologies especially for fine scale interconnections. ACFs provide unidirectional conductivity in the z-axis direction and insulation in the pitch direction (x-y direction) (Bernassau 2010).

Epoxy resin is normally used as the adhesive resin in ACFs, as it can provide a stable connecting environment and bonding between the device and substrate (Woon-Seong Kwon 2004). The silver coated polymer powders are most commonly

used as conductive particles in ACFs because they have relatively low cost and good conductive properties. The diameter of the conductive particle in an ACF depends on the pitch size of the device and electrodes (the diameter of conductive powder must be much smaller than the pitch size of the device). The finer the powder, the higher the cost. The minimum pitch size of ACFs available commercially is 50 μm, which is larger than the requirement of high frequency ultrasonic transducer devices (20 μm) (Woon-Seong Kwon 2004).

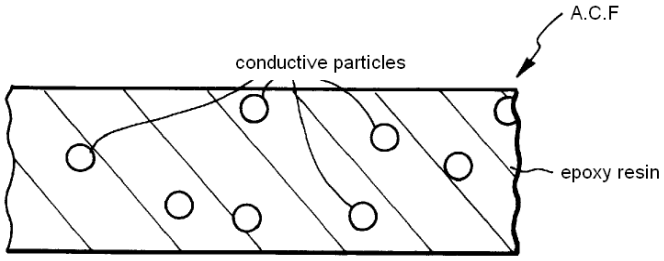

Figure 3: Cross section of ACF the conductive particles is doped in the isolative epoxy resin (Terasaka et al 1998).

2.2. Bonding Process of ACF

The ACF is placed between the electrodes, as shown in Figure 4. Under certain conditions of temperature and pressure, the electrodes are connected in the vertical direction by the conductive particles in the ACFs (Terasaka et al 1998). A typical bonding temperature is about 180℃ under an applied pressure of 150MPa and hold time of 30 seconds (J.H. Zhang 2003). During the bonding process, heating can accelerate the curing of the epoxy resin. Different types of epoxy resin require different bonding temperatures and times; the bonding pressure and conductive particle concentration are the main factors which influence the electrical conductivity of the ACF (J.H. Zhang 2003).

ACFs are also used in IC (integrated circuit) chips with conductive bumps (Au/Ni bump, 20-50 μm height, 30-50 diameter with 50 μm space), which have been deposited on an insulating substrate (Si wafer) coated with Au electrodes and connected to external circuitry. (J.H. Zhang 2003)

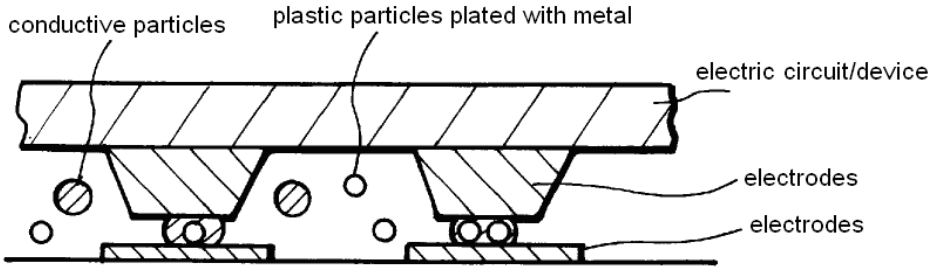

Figure 4: Sketch of the ACF interconnection. Conductive particles and plastic particles (plated metal) are compressed by the electrodes (Terasaka et al 1998).

2.3. Requirement of the ACF Interconnection

The most important properties of an ACF are electrical resistance and anisotropic electrical conductivity. The electrical resistance of an ACF should be low enough to provide a good and reliable interconnection of the device, typically the electrical resistivity is 50Ωm. The magnitude of electrical resistance is mainly influenced by bonding pressure and conductive particle concentration (Woon-Seong Kwon 2004). For the anisotropic electrical conductivity, the ACF should have a good interconnection in the vertical direction whilst it is insulating in the horizontal direction. The horizontal electrical resistivity is typically 10^6 times greater than the value in the vertical direction. It has been reported that five particles per pad can provide a stable contact resistance in IC/substrate assemblies with an inter-pad spacing of 50 μm (Woon-Seong Kwon 2004), i.e. a density of more than five particles per pad is required. A smaller concentration than five particles per electrode is unacceptable. A defect (fewer than five particles per electrode) occurrence probability

of less than 10^{-9} ensures a stable quality level in the electrical performance of the IC/substrate assembly. Normally, the ACF must provide stable interconnection at least for five years (Woon-Seong Kwon 2004).

2.4. Characterization for ACF

The bonding time and temperature are determined by the intrinsic properties of the epoxy resin (as it is cured). An increase in bonding temperature can accelerate the curing process of the epoxy resin，i.e. it can reduce the bonding time (Jong-Woong Kim.2006). Differential Scanning Calorimetry(DSC) isothermal scanning method can be used to identify the bonding time and temperature. The sample of un-cured epoxy resin is heated at different temperatures. In DSC, the exothermic peak can be recorded when the cross link reaction takes place in the resin at a certain time, this time is defined as the curing time (Jong-Woong Kim.2006). The curing state can also be easily identified by direct observation, according to the state of epoxy resin from liquid into solid state. Compared to DSC, direct observation of the surface morphology of cured epoxy resin is easier. Of course, the DSC can detect the exact bonding temperature and time.

Bonding pressure is determined by the elastic modulus of the conductive powder and the electrode bumps. A suitable pressure should be applied to deform the conductive particles enough to create a good contact between the electrodes (or bumps) and the particles. If the conductive particle deforms in an elastic manner when the applied pressure is low, the electrical resistivity will decrease as the pressure is increased.

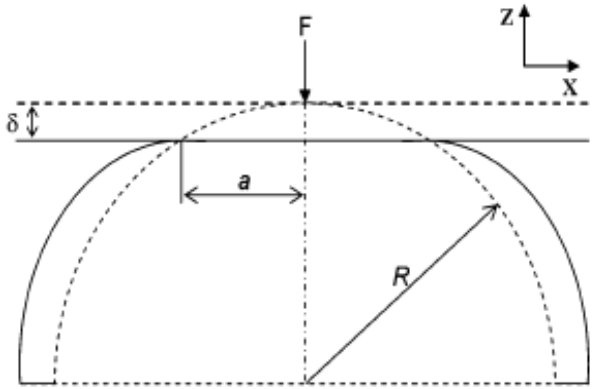

Figure 5: Schematic deformation of a half conductive particle when a contact load is applied (Woon-Seong Kwon, 2006).

Figure 5 shows the deformation of a conductive particle under a contact load *F*, the load causes an elastic deformation δ, where *a* is the radius of contact area (the contact area can be assumed as a circle), *R* is the radius of the conductive particle. By the Hertz's contact theory as presented in Woon-Seong Kwon's paper (Woon-Seong Kwon 2006), the elastic deformation induced by the contact load F can be shown as below,

$$\delta = \left(\frac{9}{16} \frac{F^2}{RE^2} \right)^{1/3} \qquad \text{(Equation 1)}$$

Where *E* is the effective modulus, *F* is the applied force on a single conductive particle.

$$\frac{1}{E} = \frac{1-\nu_p^2}{E_p} + \frac{1-\nu_b^2}{E_b} \qquad \text{(Equation 2)}$$

In equation 2, *p* means conductive particle, *b* means bump (electrode), *E* is the elastic modulus, *v* is the poisson's ratio.

Where elastic contact radius *a* is given by:

$$a^2 = R\delta \qquad \text{(Equation 3)}$$

Therefore:

$$a = \left(\frac{3FR}{4E}\right)^{\frac{1}{3}} \qquad \text{(Equation 4)}$$

$$A = \pi a^2 = \pi\left(\frac{3FR}{4E}\right)^{\frac{2}{3}} \qquad \text{(Equation 5)}$$

Where *A* is the elastic contact area (Woon-Seong Kwon, 2006).

From Equation 5, we know that increasing the load will increase the contact area, in other words, the effective conductivity of a single conductive particle is increased because of the elastic deformation of particle. So the electrical resistance is decreased as the load is increased.(Woon-Seong Kwon, 2006).

If the deformation of the conductive particle is beyond its plastic region, a crack may form on the conductive particle, which will weaken the contact between conductive particles and electrode bumps. This results in an increase of the electrical resistivity of ACF. Therefore, under high bonding pressure conditions, the electrical resistivity will increase as pressure is increased.(Woon-Seong Kwon, 2006).

The conductive particle concentration also directly influences the conductivity of the ACF, and there is an inverse relationship between the conductive particle concentration and resistivity of ACF. As the conductive particle concentration increases, the effective contact area of ACF also increases, so under the same bonding conditions, an ACF with high particle concentration will give a lower electrical resistivity (Woon-Seong Kwon 2006).

The effect of pressure and powder concentration on the ACF resistance has been investigated, The ACF samples were bonded at different pressures or different

conductive particle concentrations. The electrical resistance of the samples decreased as the pressure was increased, the electrical resistance also decreased as the powder concentration decreased, as shown in Figure 6 (Jong-Woong Kim 2006).

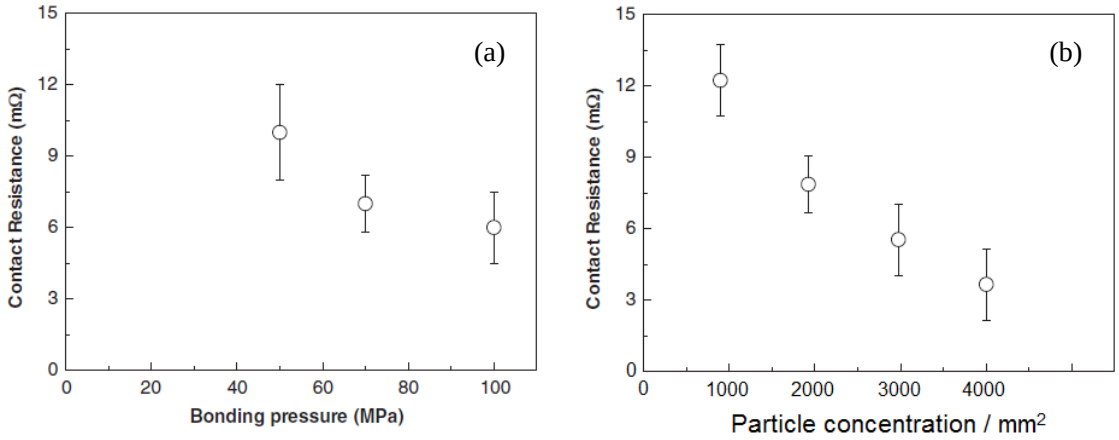

Figure 6: (a) Effect of bonding pressure on electrical resistance of ACF (b) Effect of particle concentration on electrical resistance of ACF(Jong-Woong Kim.2006).

Scanning electronic microscopy (SEM) and optical microscopy are often used to analyze the microstructure and morphology of ACF joints (Jong-Woong Kim.2006).

The applied pressure of the bonding process of ACFs may induce internal stresses in the epoxy resin film of the ACF (Jong-woong Kim 2006). The internal stress in the epoxy film sometimes leads to defects such as gap or delamination as shown in Figure 7, especially when the ACF is used for a long time such as 10 years (Jong-woong Kim 2006).

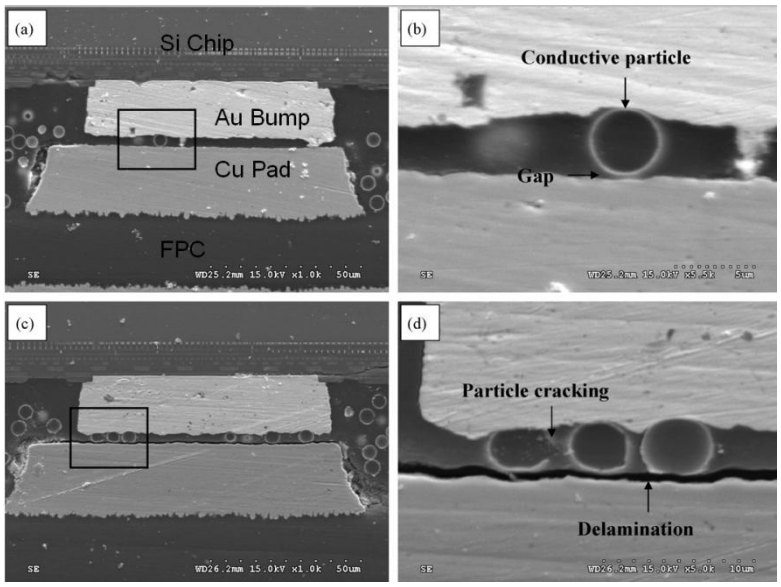

Figure 7: Cross-section view of ACF joints (Joog-woong Kim 2006).

For morphological observation of the ACFs, glass substrates are used instead of normal substrates, so that the morphology of ACF joint can be easily observed without any cutting process (Woon-Seong Kwon.2006). Typical samples are shown in Figure 8.

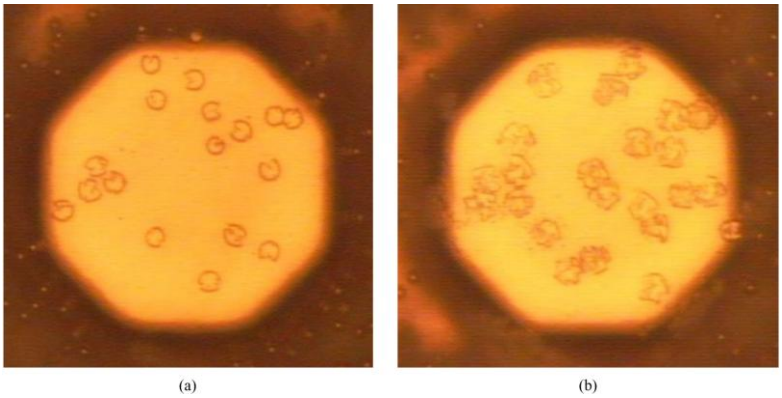

Figure 8：Optical morphology of deformed conductive particles. The crack of the conductive particle's coating layer could be observed in the pictures. Samples with same particle concentration, bonded at 180℃, hold 20 seconds. (a) applied pressure is 100MPa, (b) applied pressure is 200 MPa (Woon-Seong Kwon 2006).

As the electrical resistance will change as its microstructure gradually changes during the service of the ACF, the reliability of ACFs is also a very important factor to evaluate. The reliability and the behavior of the ACFs during service need to be characterized. J.H.Zhang has developed two methods to characterize the reliability of the ACF (also called an ageing test) (J.H. Zhang 2003): (1) high temperature and high relative humidity (RH) condition (85℃/85%) for 700-1000 hours. (2) -10℃ to 80℃ air-to-air cycling for 600 cycles, hold 30 min at the higher and lower temperatures, and the transition time between higher and lower temperature is 2 min. The electrical resistance of the ACF is measured before ageing and at different cycles. The electrical resistance of the ACF is measured at different times of 0, 50, 100, 200, 400, 700h respectively or cycles of 0, 50, 100, 200, 600 cycles respectively (J.H. Zhang 2003). These two methods of reliability tests for ACFs simulate the service time of ten years in normal working environment (room temperature/40-60% RH). The relationship between the electrical resistance of an ACF and the service time is shown in Figure 9 (J. H. Zhang 2003). The sample's bonding conditions are as followed: temperature is 200℃, pressure is 200MPa, time is 15s, particle concentration is 3500/mm^2, the conductive particles are3.5μm diameter silver coated polymer powder, the electrode bump is Al.

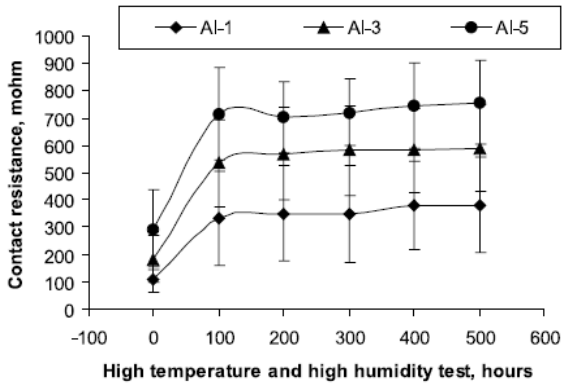

Figure 9: Variation of the contact resistance with test time for ACF and standard deviation of ACF using bare aluminum pads at 85℃/85% RH (Al-1, for 1μm aluminum pads; Al-3, for 3μm aluminum pads; Al-5, for 5μm aluminum pads).

2.5. Different Types of ACFs

Many types of ACFs have been developed already and applied in many fields, for example in interconnection of LED (light emitting diode), LCD (liquid crystal display) and other semiconductor devices. The most commonly used type of ACF has been mentioned previously and shown in Figure 3. Another type of ACF is shown in figure 10. The conducting particles are aligned in the adhesive resin film and connecting the electrodes in z-direction. The aligned fine-scale ferromagnetic conductive particles (diameter is about 1μm) provide the connection through the thickness and avoid short-circuit between the neighboring electrodes (minimum pitch size is 5μm).

During the bonding process, the ACF is heated above the glass transition temperature of the resin. Meanwhile a strong magnetic field is applied along the z-axis, and makes the conductive ferromagnetic particles align along the z-axis resulting in the anisotropic conduction in the ACF.

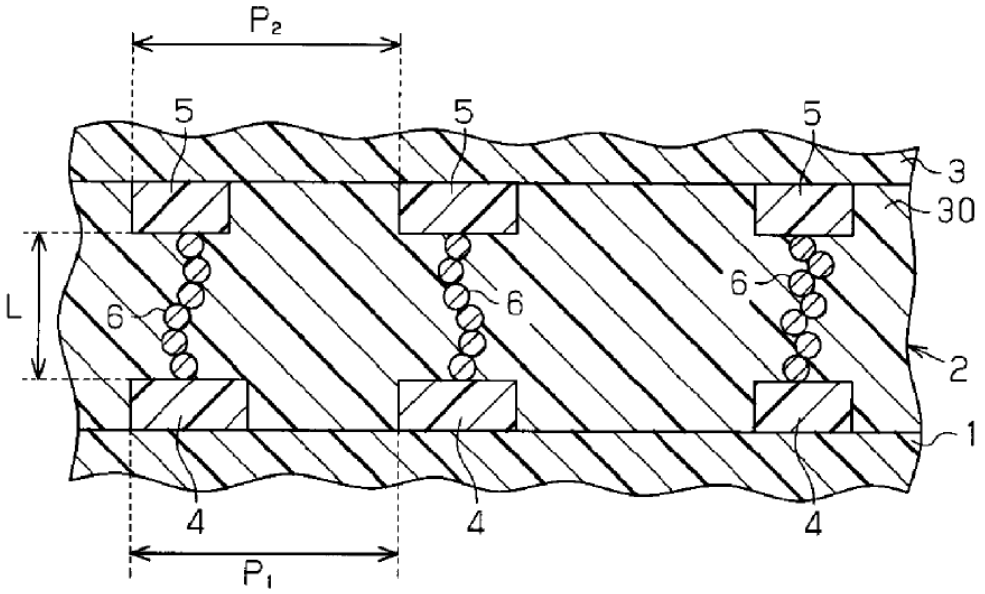

Figure 10: Cross section of ACF. (1 and 3 - the device, 2 - the ACF, 4 and 5 - electrodes, 6 - conductive particles, 30 - the thermal set polymer, L - the thickness between the electrode, P1 and P2 - the pitch width) (Yamamoto et al 2010).

.

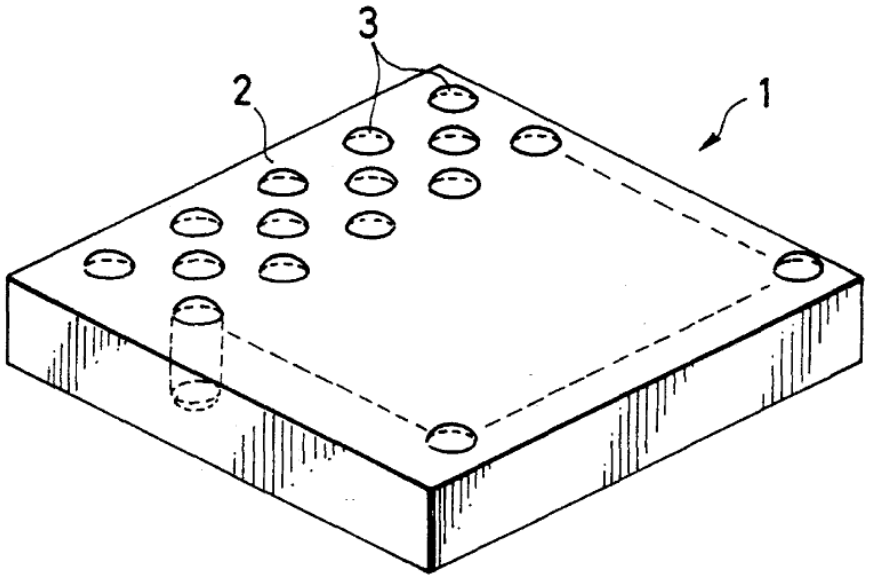

Figure 11: ACF from Maeda et al. (1 - the ACF, 2 - isolative polyamide film, 3 - the conductive silicone resin or conductive particles) (Maeda et al 1997)

Maeda et.al developed an anisotropic conductive film (ACF), which is shown in Figure 11. A matrix of conductive silicone resin is mixed with an isolative film. Compared to other types of ACFs which are shown in the previous figures, the advantage of this type of ACF (Figure 11) is that it can provide a good alignment of all the conductive particles, and totally avoid the short-circuit or isotropic conduction of the interconnection, But this type of ACF has a much more complex fabrication route than other types of ACF (Maeda et al 1997).

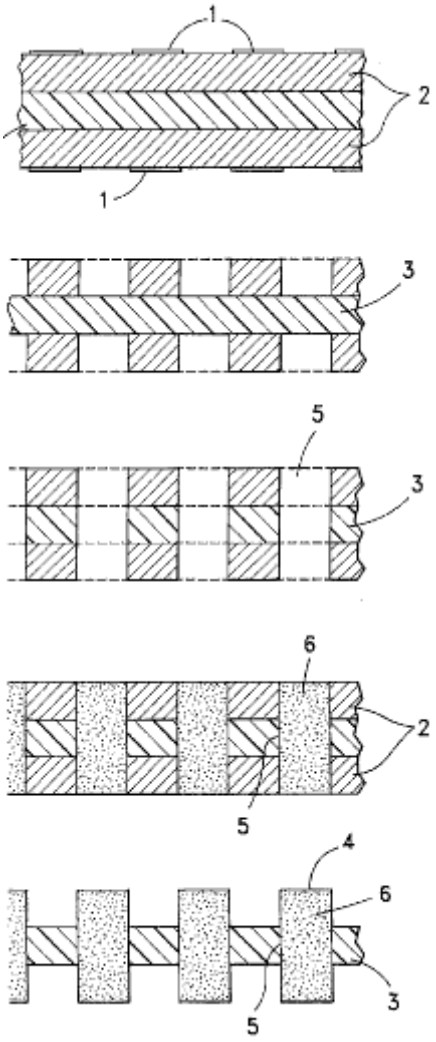

Figure 12: The manufacturing steps of the ACF is shown in Figure 11.(1- resist, 2 - the copper foil, 3- polyamide film, 4 - the gold plate, 5 - the through-hole, 6 - silicone resin) (Maeda et al1997).

The fabrication route in Maeda's method is separated into 5 steps as shown in Figure 12. Firstly, a polyamide film is prepared as an insulating film, with a thickness of about 25 micron; an approximately 17 micron thick copper foil with a resist on both sides of the polyamide film is then deposited, this copper foil is used to modify the height of the conductive bars. After these preparations, the copper foil will be etched by chloride solution to make a set of holes (diameter is 3-5μm) in the film. Through-holes are then etched with a strong alkali. The silicone resin is filled into the through-holes, and then the rest of copper foil is removed by etching. Finally a gold

layer is plated on the silicone resin to reduce the electrical resistance at the contact points. Figure 13 shows the schematic assembly of the ACF in a device. Normally, this type of ACF can be used in applications with a pitch size about 10μm.

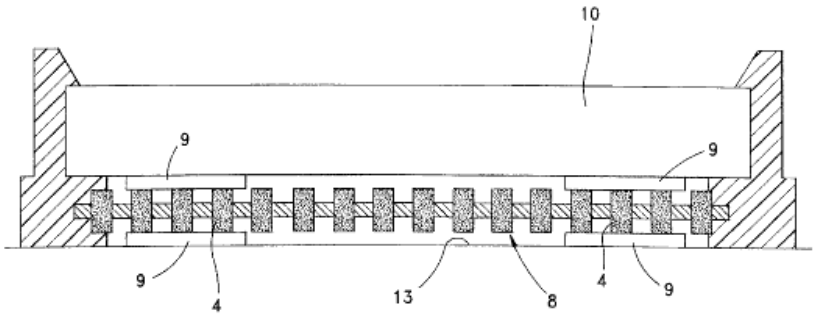

Figure 13: Cross sectional view of a semiconductor device being electrical connected with a substrate via anisotropic conductive film. (4 - conductive polymer bars with 5μm diameter, 8 - ACF, 9 - electrodes, 13 and 10 - device with 10μm minimum pitch size) (Maeda et al 1997).

2.6. Objectives

Ultrasonic transducers are widely used in many fields. For improving the resolution the array type high frequency ultrasonic transducers are used, which requires fine scale interconnections, for example 20μm pitch size interconnection device. Therefore the ACF is the best choice. The minimum pitch size of commercially ACF available for purchase is 50μm. The aim of this study is to prepare an ACF which is suitable for high frequency ultrasonic transducers and which can be synthesized from conductive particles and epoxy resin. The conducting mechanism of the interconnection, the influence of parameters including the production route, content of conductive powders and microstructures of the prepared ACF will also be studied. Finally characterization of the ACF will be carried out in order to optimize the performance of the prepared ACF.

3. Experiments

3.1. Materials Selection

The raw materials used in the experiments are EPOFIX and the silver coated copper particles.

The EPOFIX (Struers Ltd.) contains two components: epoxy resin and hardener (Triethylenetetramine). They are purchased from Struers Ltd. The weight ratio of epoxy resin: hardener = 25:3 was determined according to our group's previous work (Struers Ltd. manual),.

The silver coated copper powders (Quatan-Nano Ltd Co. Hefei, China) were chosen as the conductive particles in the ACF. The composition and the physical properties of the conductive powder are shown in Table 1.

The particle size distribution was measured by laser particle size analyzer (SYMPATEC Ltd.) as shown in Figure 15. 0.5g of conductive powder was mixed with 1g of dispersant (Sodium hexametaphosphate) and 10g distilled water. After a uniform mixture was prepared, the samples were put into the chamber of the particle size analyzer equipment. The particle size distribution of the silver coated copper powders was shown in Figure 14. The average particle size is 7μm (D50 means the particle size of powders when the cumulative distribution is 50%), D10 is 3μm, and D90 is 50μm.

Table 1: The composition and physical property of the silver coated copper powder

Ag (wt %)	Cu (wt %)	Resistivity（ohm/cm^2）	shape
z23	77	0.015~0.025	sphere

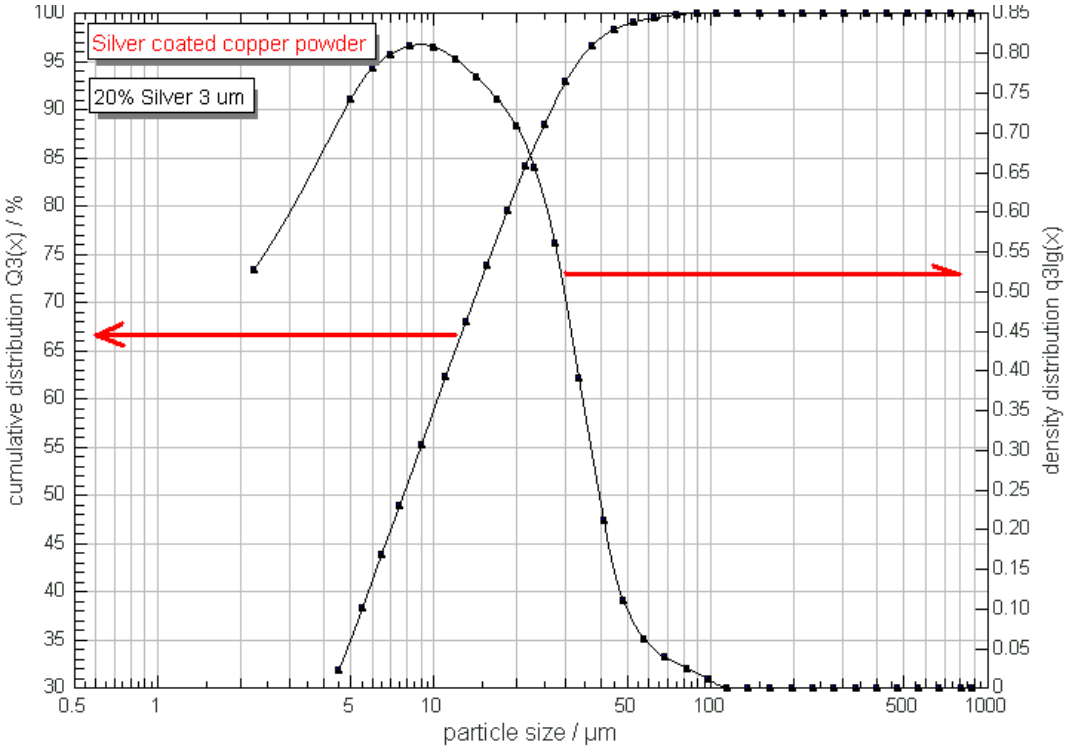

Figure 14: The particle distribution of silver coated copper powder

Figure 15: Laser particle size analyzer (SYMPATEC Ltd.)

3.2. Experimental Procedure

3.2.1. Epoxy Resin Film Tape Casting and Surface Morphology Observation

Appropriate amounts of the epoxy resin and harder were weighed using an electric balance according to the ratio of 8.3:1(epoxy: harder). They were put in a glass tube and stirred by hand using a glass rod until a uniform mixture of this uncured resin was obtained

1g of uncured resin was dropped on to a prepared 5×5 cm^2 Al_2O_3 substrate (96% alumina, 50 x 50 x 1mm, Dynamic Ceramic Ltd.) on which there were two 100μm thick self adhesive plastic strips (RoHS Ltd.) attached to its two sides, as shown in Figure 16. The resin was spread smoothly on the Al_2O_3 substrate by a doctor blading technique, which is also called tape casting. The thickness of the epoxy film was about 100μm as controlled by the thickness of the plastic strip. After the tape casting, the resulting un-cured epoxy samples were stored at room temperature. The samples were used for subsequent experiment within 15 minutes of fabrication because the epoxy resin takes 12 hours to get fully cured under room temperature conditions.

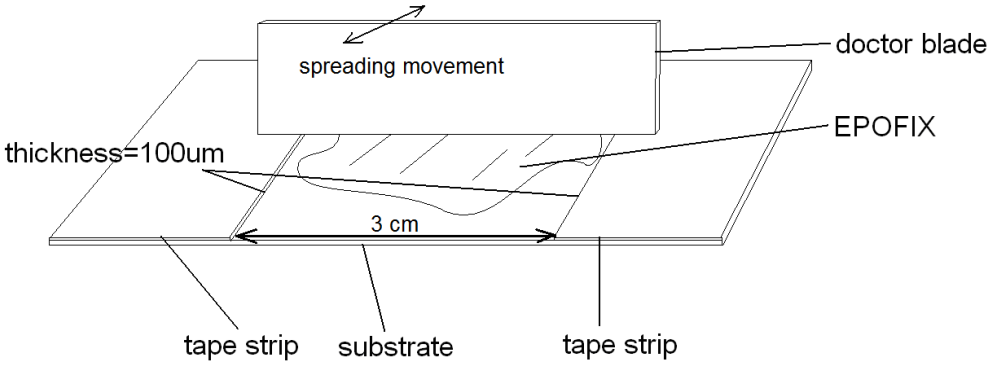

Figure 16: Schematic diagram of tape casting.

The samples were divided into 6 groups with 6 test pieces in each group. These 6 groups of samples were respectively cured at different temperatures as shown in Table 2:

Table 2: Curing temperature of different groups of samples

Group1	Group 2	Group 3	Group 4	Group 5	Group 6
80℃	100℃	120℃	140℃	160℃	180℃

All the samples were heated in an oven (Lenton Thermal Designs Ltd.), then the surface morphology of the samples were observed at every minute to identify the curing state of the EPOFIX. A glass rod was used to touch the surface of the sample to identify whether the sample changed from liquid to solid, the curing process is

finished when the whole sample is in a solid state. The data of time and temperature were recorded.

A second set of 6 groups of samples were prepared at the same temperatures as in Table 2, but the samples were covered by $3\times5cm^2$ glass slides (Propper Ltd.) to simulate the situation of a device bonded on the ACF (Figure 17).

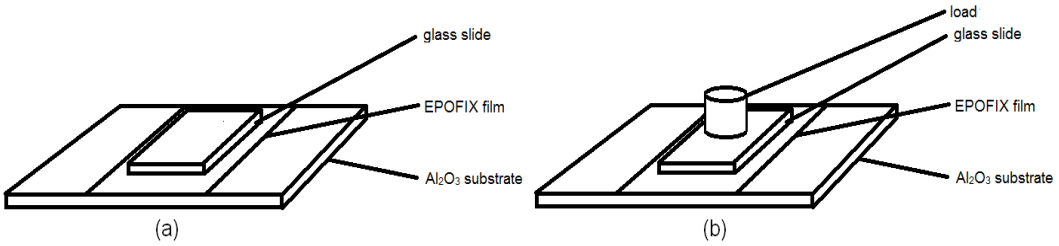

Figure 17: Schematic diagram of sample assembling. (a) Sample without pressure (b) Sample with pressure.

There were 4 samples in each group which were covered by glass slides and cured under a pressure of 50Mpa. The pressure was provided by a weight on the top of substrate as shown in Figure 17 (b), The other 2 samples in each group were cured without any pressure (Figure 17 (a)). The curing state of the samples were assessed every minute also by a glass rod as described previously.

3.2.2. Preparation of the ACF

3.2.2.1. The Preparation of Electrodes on the Al_2O_3 Substrates

As shown in Figure 18, the shaded area on the Al_2O_3 substrate (5×5 cm^2 square plate) was firstly covered by a tape strip with, the uncovered area being the electrode area. Then the samples were transported to the gold Sputter instrument (EMITECH Ltd. K575X, Figure 19) for sputtering. The substrates were sputtered with three cycles. In the first cycle, the substrate was sputtered by Cr target. In the second and third cycle, the Cr target was replaced by an Au target. The sputter current was 80 mA and

the sputter voltage was 120 mV for the three cycles. The sputtering process was maintained for 120 seconds. When the sputtering was finished, the adhesive tape strips were removed from the substrates.

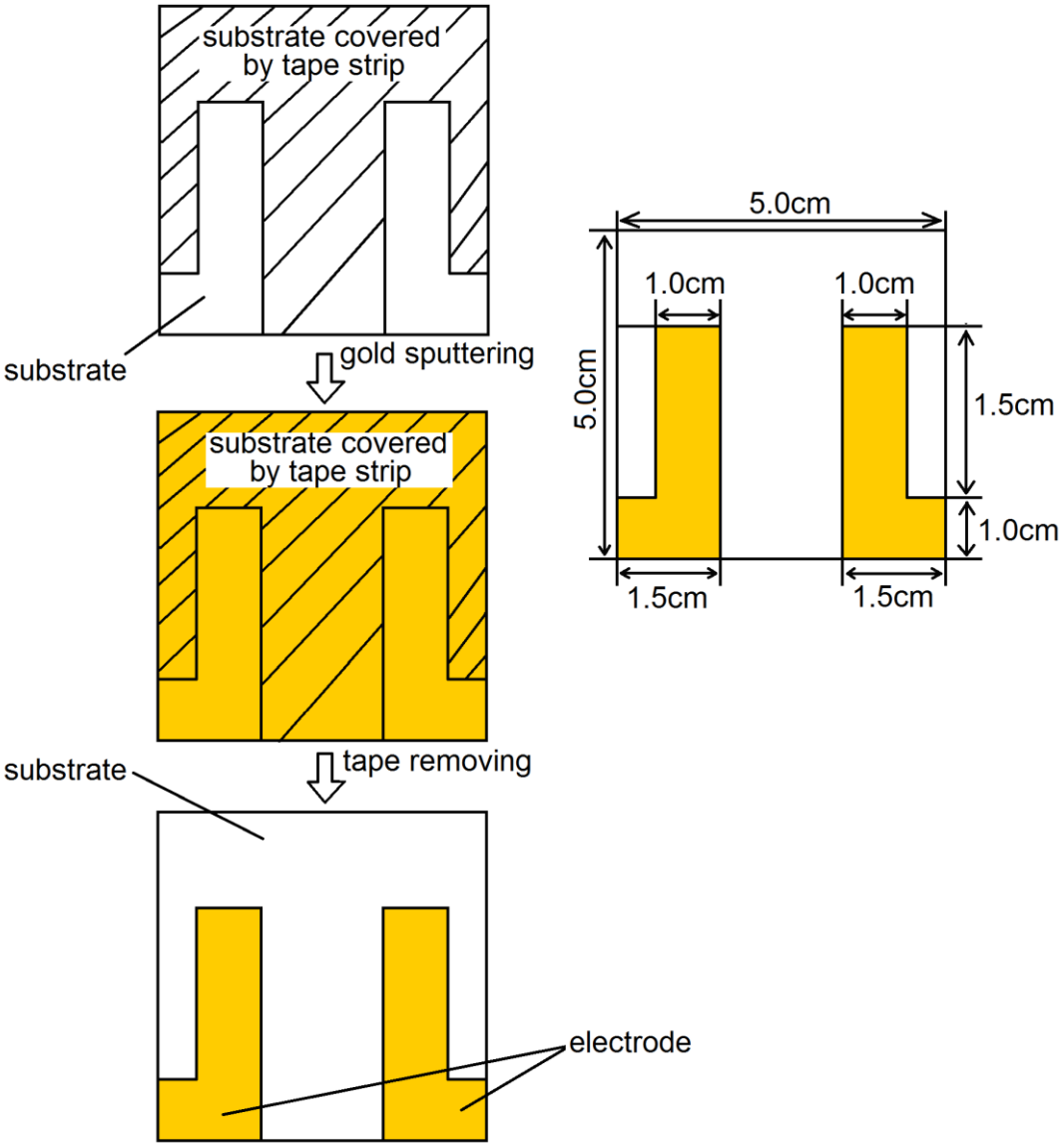

Figure 18: Schematic of the substrate preparation.

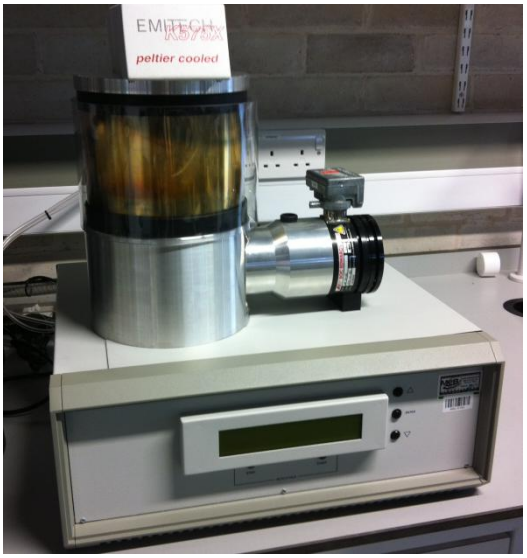

Figure 19: Gold sputtering (EMITECH Ltd. K575X)

3.2.2.2. ACF Preparation

Firstly, the uncured resin was prepared as described in section 3.2.1. The resin and the silver coated copper powder were then weighed according the ratio as shown in Table 3. Thereafter, they were put into a glass tube and stirred by hand with a glass rod for approximately 10 minutes until a uniform mixture was obtained.

1g of the prepared composite (EPOFIX resin and conductive powders) was dropped on to the Al_2O_3 substrates with Au sputtered electrodes and spread on the substrates as in section 3.2.1. Another ceramic substrate covered the systems as shown in Figure 20. 30 samples were prepared using the same method and were divided into 15 groups for investigation of the curing process. These 15 groups of samples were transferred into the oven (Lenton Thermal Designs Ltd.) and then were cured at 120 ℃for 20 minutes. Different pressures as shown in Table 4 were applied to the samples during the bonding process.

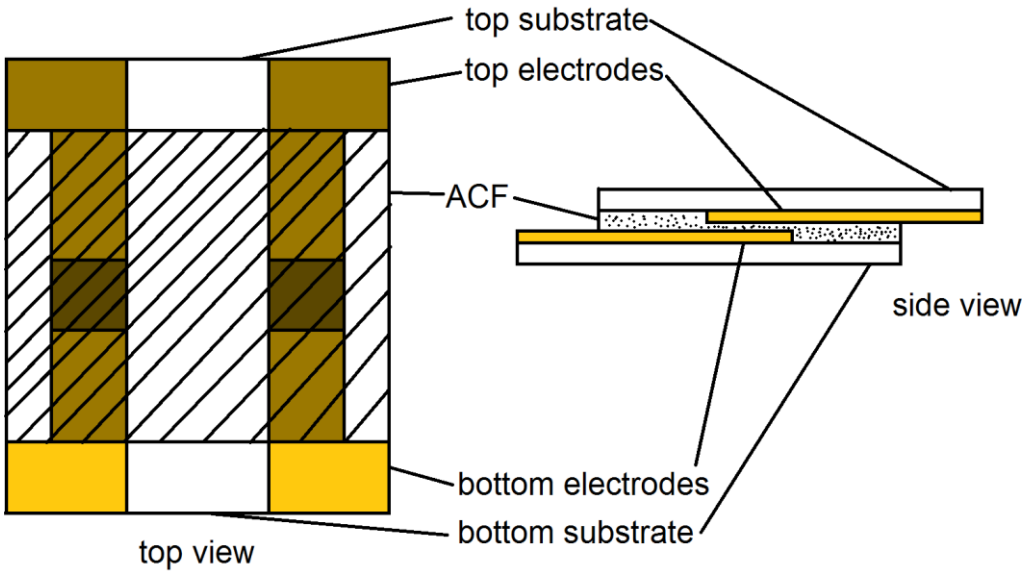

Figure 20: Schematic diagram of substrates and ACF assembling

Table 3 The conductive particle concentration in the ACF

	Group 1	Group 2	Group 3	Group 4	Group 5
particles/mm^2	350	700	1050	1400	1750
Powder wt%	2.2	4.3	6.4	8.3	10.2
	Group 6	Group 7	Group 8	Group 9	Group 10
particles/mm^2	2100	2450	2800	3150	3500
Powder wt%	12.0	13.7	15.4	28	18.5

Table 4 The applied pressure on the samples during the curing process

Group	Group 1	Group 2	Group 3	Group 4	Group 5
Pressure, MPa	0.5	1.0	1.5	2.0	2.5
Group	Group 6	Group 7	Group 8	Group 9	Group 10
Pressure, MPa	3.0	3.5	4.0	4.5	5.0
Group	Group 11	Group 12	Group 13	Group 14	Group 15
Pressure. MPa	5.5	6.0	6.5	7.0	7.5

3.2.3. Measurement of Electrical Resistance

After the bonding process was completed, all the samples were taken out from the oven and cooled at room temperature for 20 minutes. Horizontal and vertical electrical resistances were measured for each sample. The electric resistance measurement circuit is shown in Figure 21; an amperemeter and the voltmeter were used to measure the electrical resistance of the electrodes and the samples.

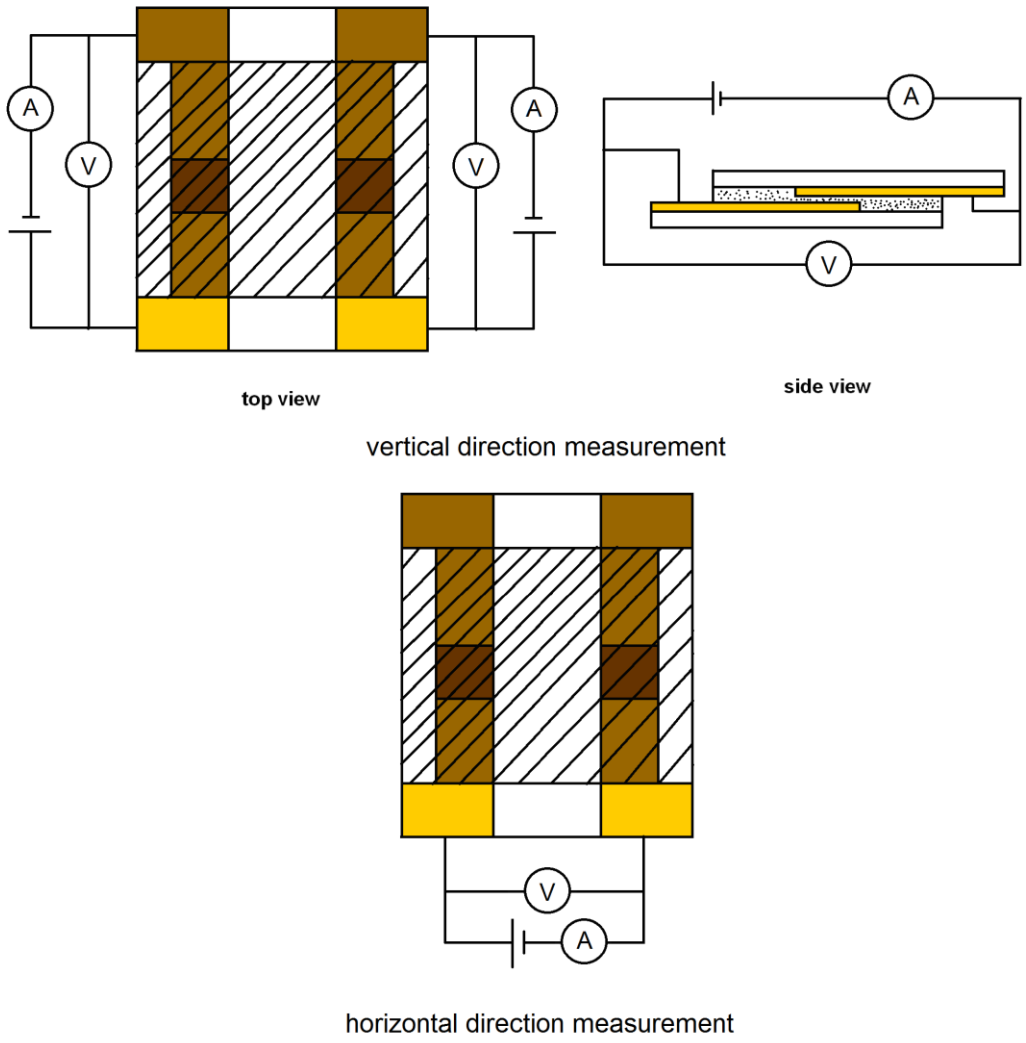

Figure 21: Schematic diagram of test circuit of electrical resistivity measurement of ACF

3.2.4. Reliability Test

The reliability test was carried out in an environmental chamber. 500g KCl saturated solution was used to produce the relative humidity (RH=80%) and an oven was used to maintain the temperature (80℃). 5 samples of group 10 in Table 3 were chosen for the reliability test. They were prepared in the same conditions: bonding temperature 120℃, bonding pressure 1.5MPa，and bonding time 20 minutes. The electrical resistance of samples were measured and recorded every 50 hours.

3.2.5. Microstructure and Morphology Observation

The microstructures of the samples were observed by scanning electronic microscopy (SEM, Philip 30) which was also utilized to observe the cross-section view of ACF joints. The accelerating voltage of the SEM was 15.0 kV, spot size was 7.0mm, and working distance was 10 mm.

An optical microscope (PME3, Olympus Ltd., Japan) was employed to observe the distribution of conductive particles between the electrodes in the ACFs. For observation purpose, a glass substrate instead of alumina substrate was used during the ACF fabrication process; the electrode pattern is shown in Figure 22. The ACF fabrication route was conducted according to section 3.2.2.2 (the bonding condition was 120℃/1.5MPa/20 minutes).

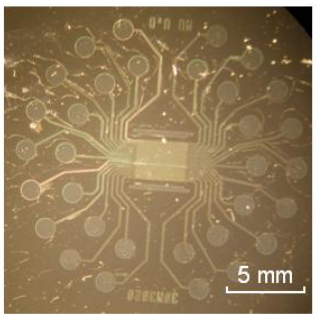

Figure 22: Electrode pattern

3.3. Experimental Data Errors

There were three main steps of this project: ACF preparation, ACF performance characterization and reliability test. Because of the intrinsic properties of epoxy resin, which would be cured at room temperature within 12 hours after mixing, the epoxy resin or ACF would be wasted if it was not used in time. Experiments were therefore separated into several days, but each time the epoxy resin mixture was prepared it could not be guaranteed that there was exactly the same mass ratio, this could influence the bonding time and life time. (J.H. Zhang 2003). During the mixing of the conductive powder and epoxy resin, there could be a variation of the mass ratio, because, in each experiment, the mass of the conductive powder is 0.23g and epoxy resin is 1.01g; those small amount mixtures led to a certain error. The difference between real particle concentration and theoretical concentration directly influences the electrical resistance of ACF.

During the bonding process, heating and pressing should applied at the same time. By the limitation of equipment, the pressure was place on top of samples before the sample was put into the oven, i.e. the pressing load was added on the sample ahead of the heating process, thus the pressing time was longer than the bonding time. As the curing process of epoxy resin needs about 12 hours at room temperature, and the curing process at high temperature is only a few minutes, therefore the load time before heating was relative short. This error of pressing time was acceptable. The cold body of the load will absorb a certain amount of the heat, which could delay the curing process of ACF.

4. Results and Discussion

4.1. Effect of Bonding Temperature on Curing Process of the EPOFIX

The bonding temperature, time and curing state of EPOFIX were recorded as

shown in Figure 23, which shows the bonding time of epoxy film at different temperatures. It is obvious that the bonding time of epoxy film decreases rapidly as the bonding temperature increases. The bonding time decreases from 12 minutes to 2 minutes as the temperature increases from 80 to 180℃. Bubbles appear in the film when the curing temperature reaches 180℃.

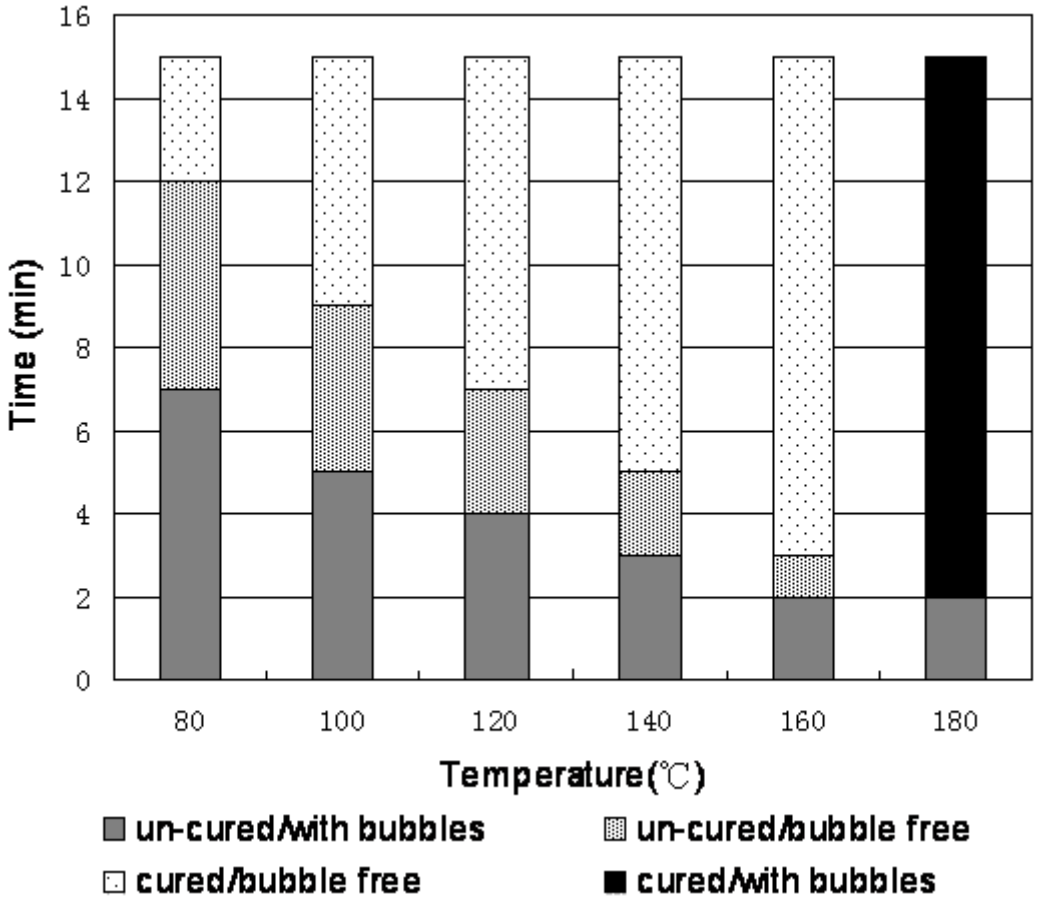

Figure 23: Relationship between the bonding time and temperature of samples

Figure 24 shows the surface morphology of cured epoxy resin samples, which have not been covered by glass slides. A few (one or two) bubbles can be observed in the whole sample when the temperature is below 180℃. The number of bubbles increases dramatically when the temperature reached 180℃. These bubbles were distributed randomly in the epoxy film and appeared to be similar in size.

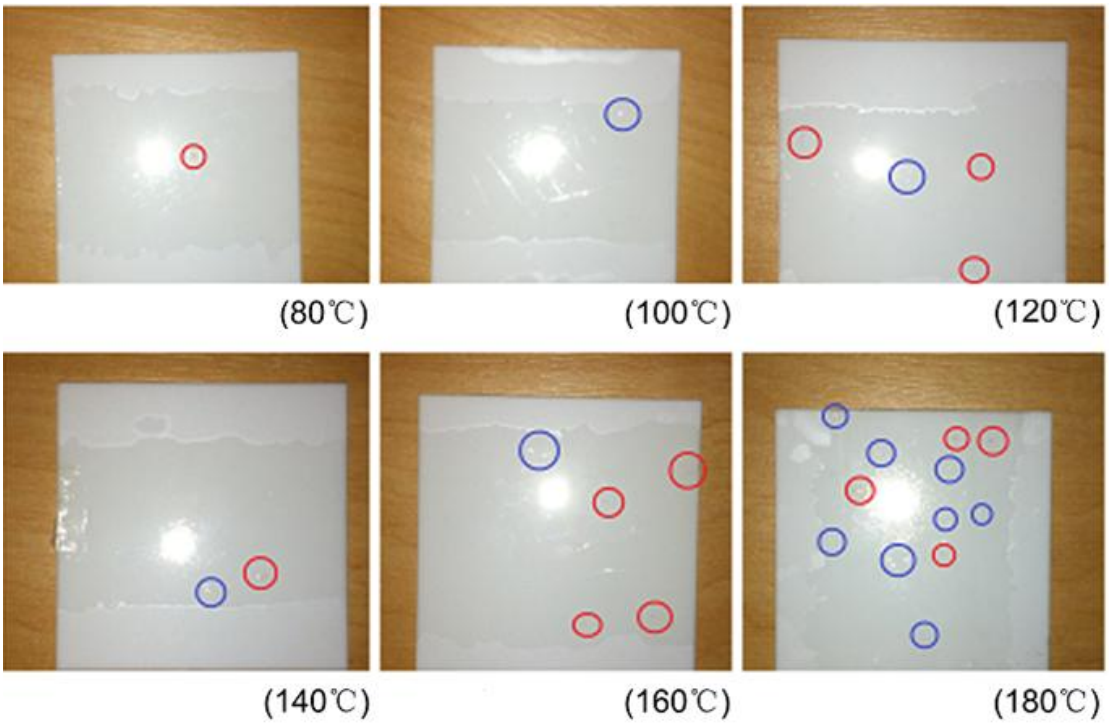

Figure 24: The surface morphology of the samples cured at different temperatures without glass slides cover. The red circles denote impurities and dirt, and the blue circles denote the air bubbles in the photos; the white spot is the reflection of light bulb.

The relationship between the cureing time and bonding temperature is also shown in Figure 25; the data of the curve is based on Figure 23. The de-airing time of the samples with increasing temperature is also shown in the figure.

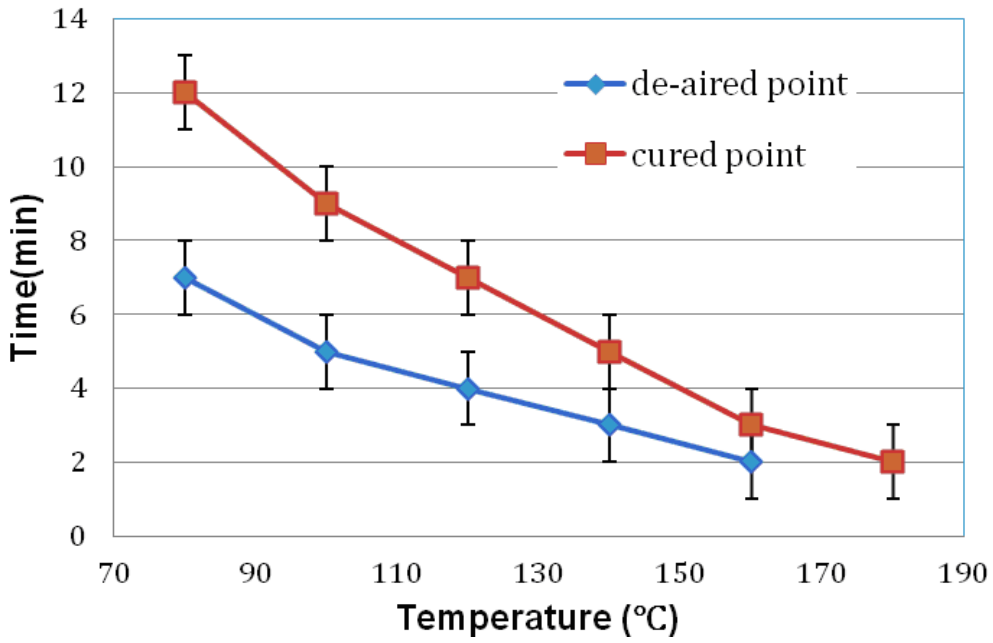

Figure 25: The relationship between the cured time and temperature of the curing state and air bubble appearance states. Samples without the glass slide cover

As shown in Figure 25, the curing time decreases as the curing temperature increases, which means that the curing process of the samples is accelerated by the temperature. When the resin and hardener are mixed, the epoxide group of resin reacts with the amine group of the hardener to form a covalent bond. This makes the epoxy molecule get heavily cross linked to form a hard and strong solid polymer (Bernassau 2010). The higher the temperature of heating, the more energy is absorbed in the sample, which helps the chemical reaction between the resin and hardener (Bernassau 2010). Therefore the curing process is accelerated. i.e. the bonding time of EPOFIX is reduced, by increasing the bonding temperature.

During the mixing of the two components, air can be easily trapped in the composite material. After tape casting process, the air still remains in the un-cured epoxy film. During the heating process, the air dispersed in the material will however be released from the epoxy film automatically. According to Figure 25, the de-airing time is decreased as the temperature increases, which means the de-air process is accelerated by the curing temperature. As we know the mobility of the gas molecules

in the solution depends on the temperature, so as bonding temperature increases, the mobility of air bubbles in un-cured epoxy film is increased; the mobility of epoxy resin molecules also increases as the temperature increases (Woon-Seong Kwon 2004). Accordingly, the air bubbles will move faster at the higher curing temperature, and this phenomenon will result in a higher de-airing rate (air bubble releasing rate) as the bonding temperature goes up. In the practical application of ACFs, the air bubbles in the cured ACF would induce a gap between the device and film, which weakens the interconnection, or could induce delamination of the ACF joint. Therefore, in the ultrasonic transducers, air bubbles should be avoided in the ACF application and the bonding temperature should be as high as possible. However, according to the data in Figure 25, the air bubbles cannot escape from epoxy film when the bonding temperature is raised above 180 ℃. Due to the high curing speed, there is not enough time for the bubbles to escape from the epoxy film before the film is fully cured. There are still air bubbles trapped in the cured epoxy film. Hence to avoid the presence of air bubbles in ACF, the bonding temperature should be around 120-160 ℃.

4.2. Effect of Pressure on the Curing Process

Figure 26 describes the sample appearance (presence of bubbles) during the curing process and the relationship between curing temperature and time for the samples covered by glass slide with pressure and without pressure, respectively. From Figure 26, it can be concluded that: 1) the curing time decreases as temperature increases gradually for the samples with pressure or without pressure. In omparison to the data shown in Figure 23, the curing time of the samples with glass slide cover is little longer. 2) The cured time of the samples were delayed by the applied pressure at the different curing temperatures. 3) The applied pressure can help the bubbles escape from the samples.

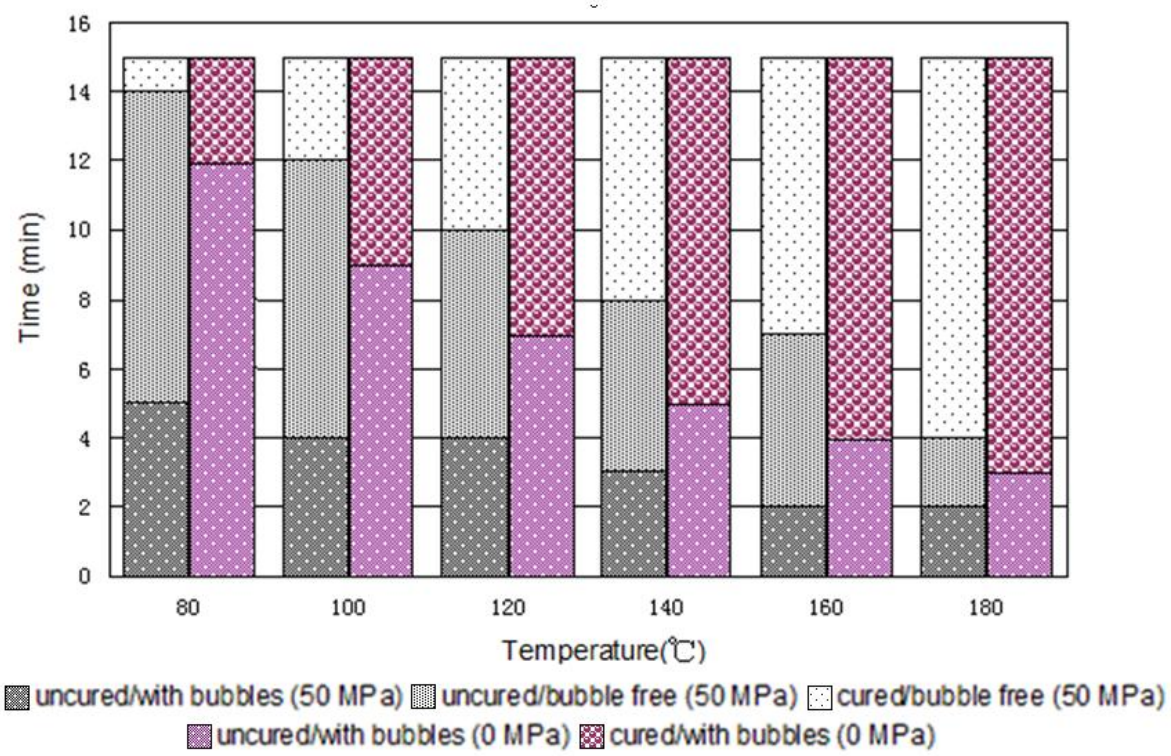

Figure 26: The state of samples varies with curing temperature and time. The samples were covered by glass slide (pressure is 50MPa)

Figure 27 are the photographs of samples covered by glass slides but without pressure. A large number of bubbles is easily observed on whole surface of every sample cured at all the temperatures, the size of bubbles is much larger than the ones in the samples without glass slide covers (as shown in figure 24). Obviously, the bubbles were interrupted by cured resin located in the edge of the glass slide, i.e. the epoxy resin in the edge area of the glass slide may cured ahead of the center area of the glass slide, therefore, the bubbles could not break through the "cured resin wall" and remain in the films.

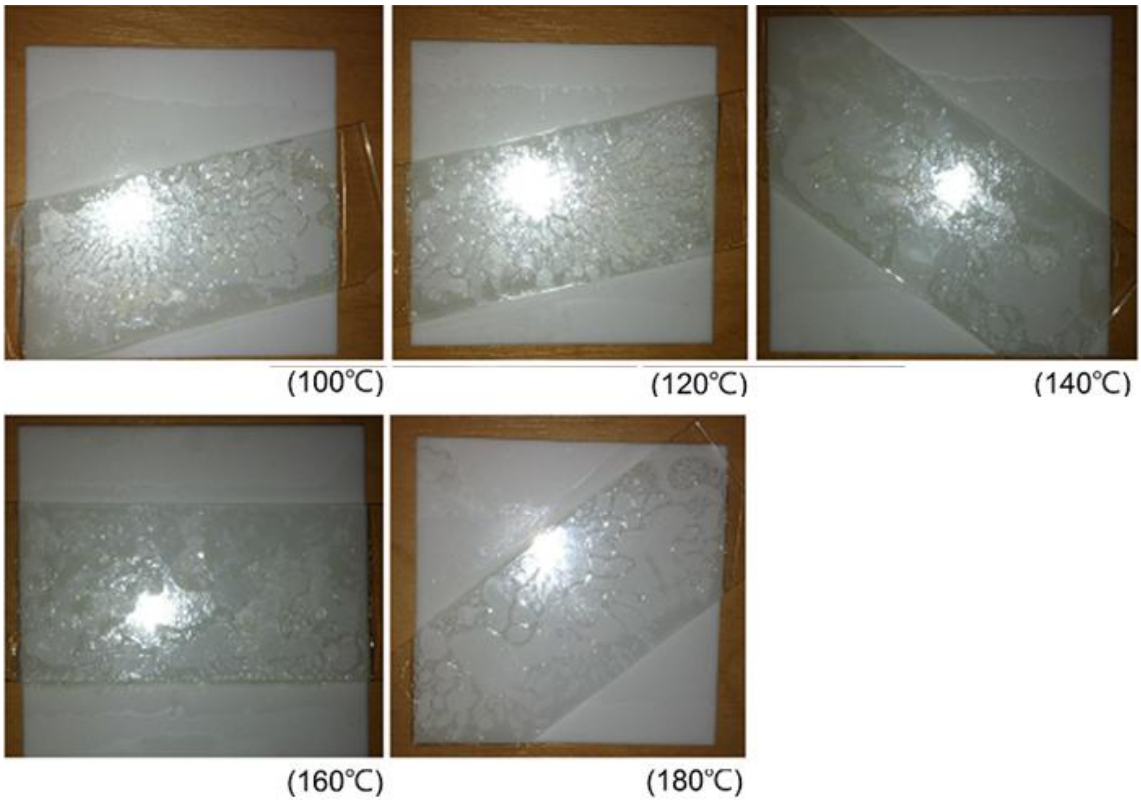

Figure 27: The surface morphology of the sample with glass slides cover without pressure at different cured temperatures. The white spot is the reflection of light bulb.

Figure 28 shows the surface morphology of samples covered by glass slides under a pressure of 50MPa. Bubbles can be found on the whole surface of the samples cured at different temperatures.

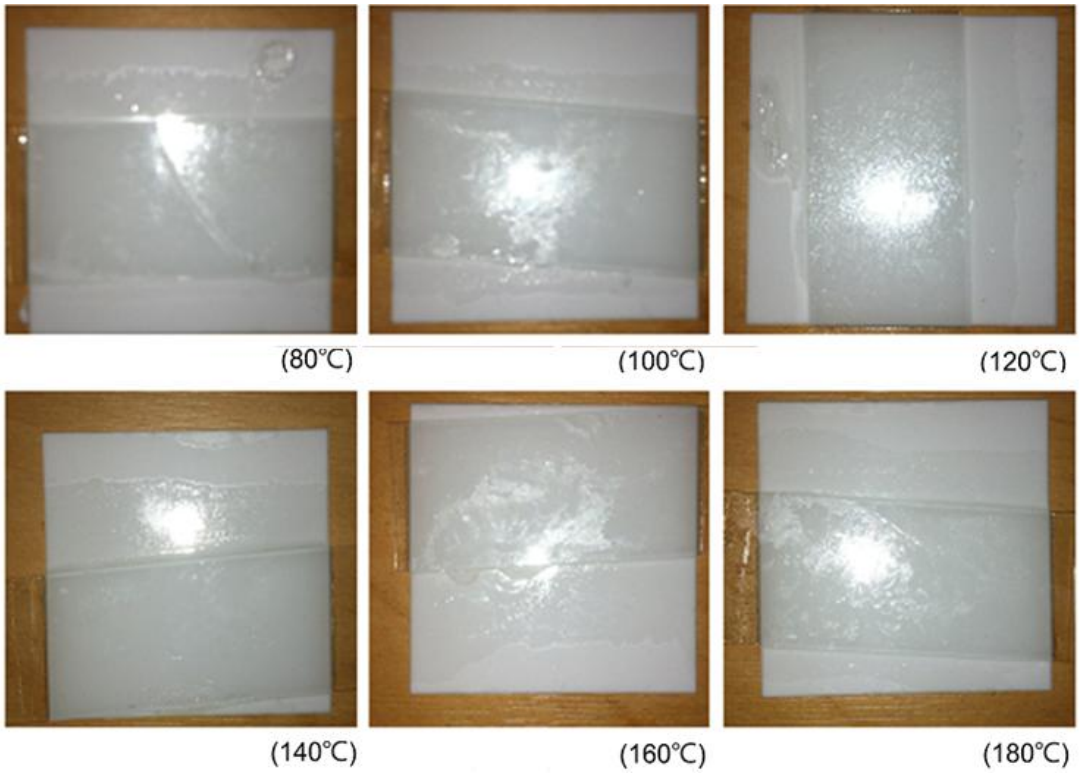

Figure 28: The surface morphology of the sample cured at different temperatures with glass slide cover under pressure of 50MPa, the white spot is the reflection of light bulb.

Figure 29 shows the relationship between the curing times and curing temperatures of the EPOFIX under pressure. And the data of the curve is based on Figure 26. Comparing the pressed curve and un-pressed curve in Figure 29, it is obvious that the applied pressure enhances the curing process of the epoxy resin.

The curing process is mainly affected by the curing temperature for the same materials of epoxy resin. While the samples are heated in an oven, it needs time to heat the whole sample and load body from room temperature to the curing temperature. For the pressed samples, besides the glass slide, there is extra volume of the load body on the top of it. Hence, a longer time is needed to heat the pressed samples to the same curing temperature than un-pressed samples. This is the one of

the reason why the curing times of pressed samples are a little longer than those of the samples without pressure. Another factor affecting the curing process is the atmosphere. The glass slide covering the surface of the epoxy resin film reduces the contact area of film-to-air, as a result, the oxygen cannot diffuse into the epoxy and then the chemical reaction of curing process is delayed (Michael J. Adamson 1980).

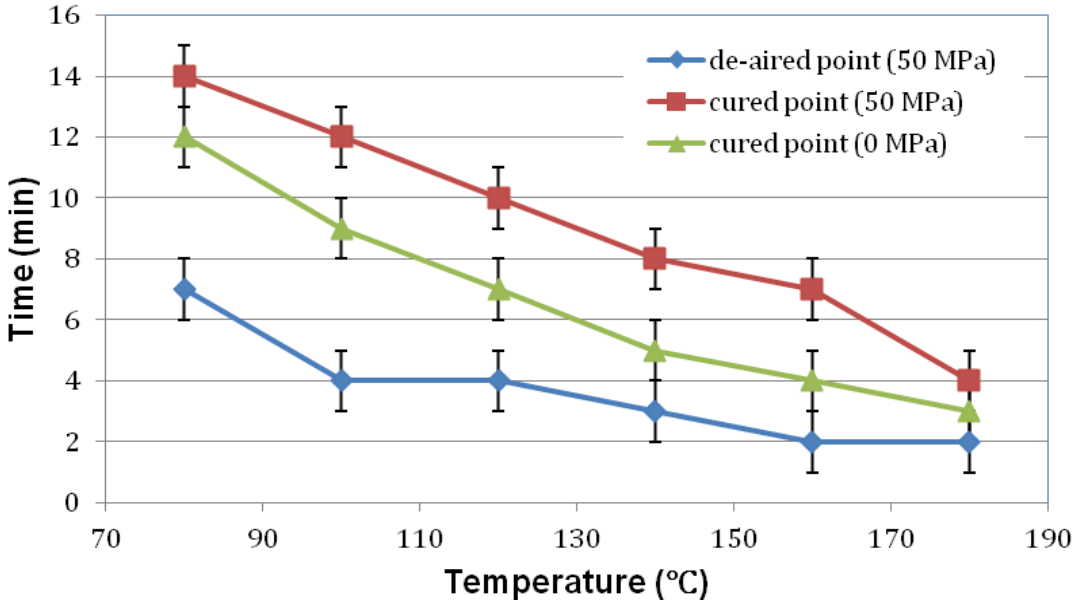

Figure 29: The relationship between the time and temperature of the curing state and air bubble appearance states, all samples covered by glass slide.

Comparing Figures 25 and 29, it can be concluded that the de-airing rate of the sample with pressure is higher than that of the sample without pressure, i.e. the applied pressure can help the escape of air bubbles from the curing resin film. Naturally, the bubbles will easily escape from the surface of the resin film during the curing process because the thickness of the film is small. As the un-cured resin film is covered by the glass slide, the bubbles formed from the resin film during the curing process were also covered on the surface of the cured resin film or underneath the glass slide (i.e. between the film and the glass slide). As a result, a large numbers of bubbles are observed in Figure 27. In fact, further observation was taken during the curing process. The epoxy resin is cured faster at the edge of glass slide than that at the central area of glass slide because of the oxygen diffusion. Actually, the cured

epoxy resin forms a wall at the edge of the glass slide to prevent the air diffusion from the edge into centre area and hence the bubbles are trapped in the gap between the wall, i.e. between the resin film and the glass slide. When the pressure is applied on the glass slide of the samples, the internal pressure of the bubbles is increased and they are forced to be released from the sample. There are no bubbles left in the pressed samples, while there is a large number of bubble left in the samples without pressure, because not enough force is exerted to make the bubbles escape from the film. This phenomenon was also found in the work by Michael J. Adamson et al. (Michael J. Adamson 1980).

4.3. Effect of Pressure on Electrical Resistance

Figure 30 depicts the variation of the vertical electrical resistance with pressure applied during curing at 120℃. The electrical resistance decreases as pressure increases when the pressure is lower than 1.5 MPa, then increases when the pressure is in the range of 1.5 MPa to 2.5 MPa. At higher pressures (2.5MPa to 6 MPa), the curve is a plateau and a minimum electrical resistance of 0.5Ω is observed at a pressure of 1.5 MPa.

In Figure 31, it can be seen that the horizontal electrical resistance changes randomly against the pressure increase and the value of the resistance is much larger than the result shown in Figure 30.

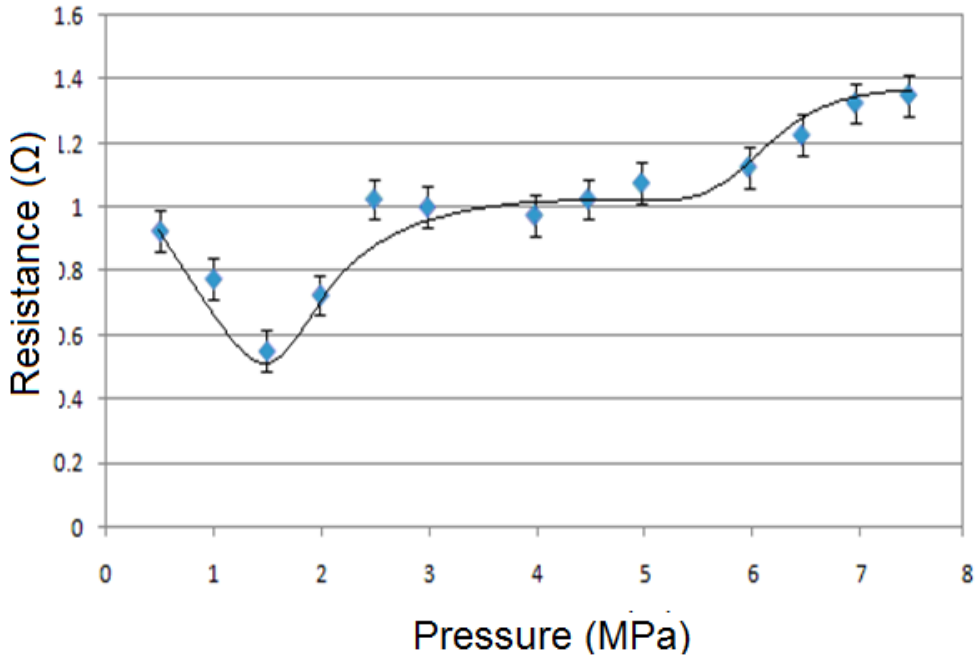

Figure 30: Relationship between the electrical resistance and pressure applied on the ACF. The data points were taken from the average electrical resistance under different pressures and the curve is trend line.

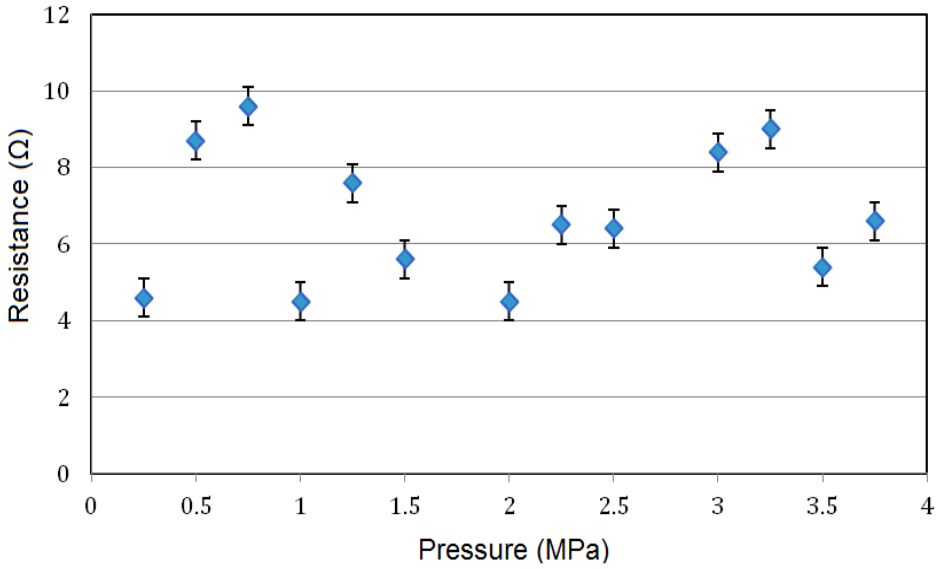

Figure 31: The relationship between horizontal electrical resistance and pressure applied on the surface of ACF.

As shown in Figure 30, at the beginning, the resistance decreases from 0.9Ω to 0.5Ω as the pressure increases from 0.5 MPa to 1.5MPa. The pressure enhances the connection between the electrode and conductive particles dispersed in the ACF, especially underneath the surface of the ACF. This phenomenon is displayed in Figure 32 and Figure 33. With low pressure, large agglomerated powders play the main role in the interconnection of ACF. However, as the pressure increases, the deformation of those agglomerated powders increases too, which results in an increasing effective contact area. Deformation is increased from Figure 32 to 33. Therefore, during the initial period, the electrical resistance of the sample decreases.

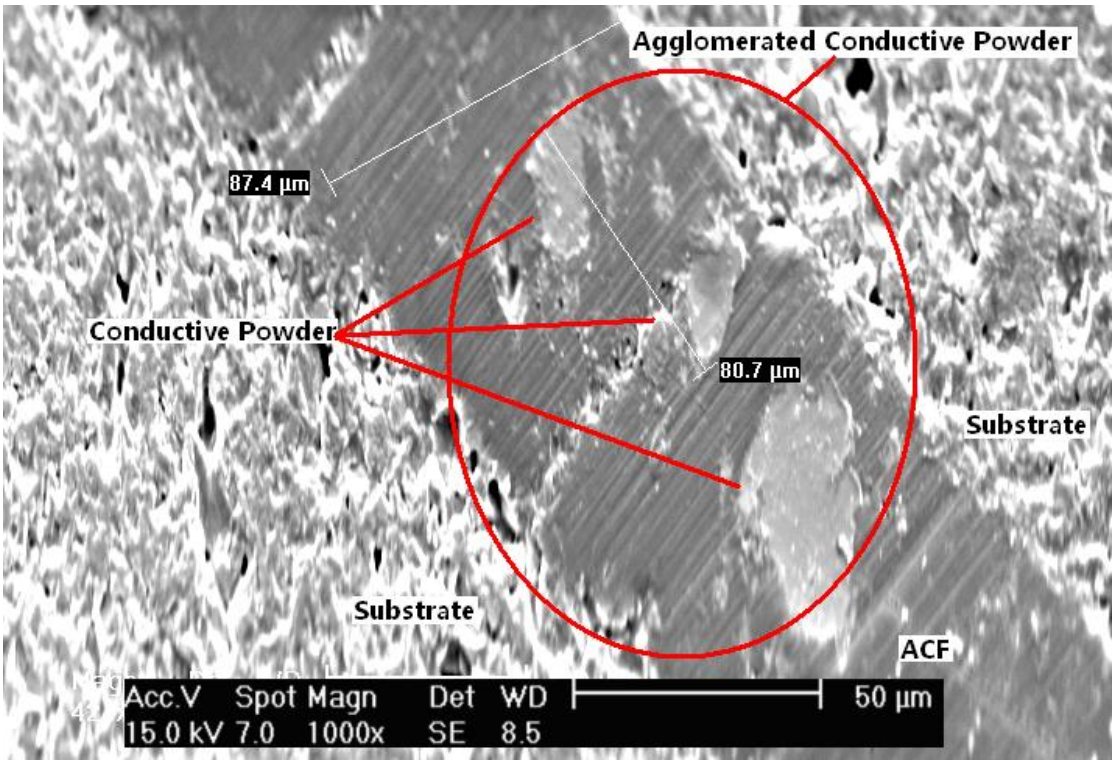

Figure 32: The cross-section of ACF joints bonded under pressure of 0.5MPa, the agglomerated conductive powder is labeled.

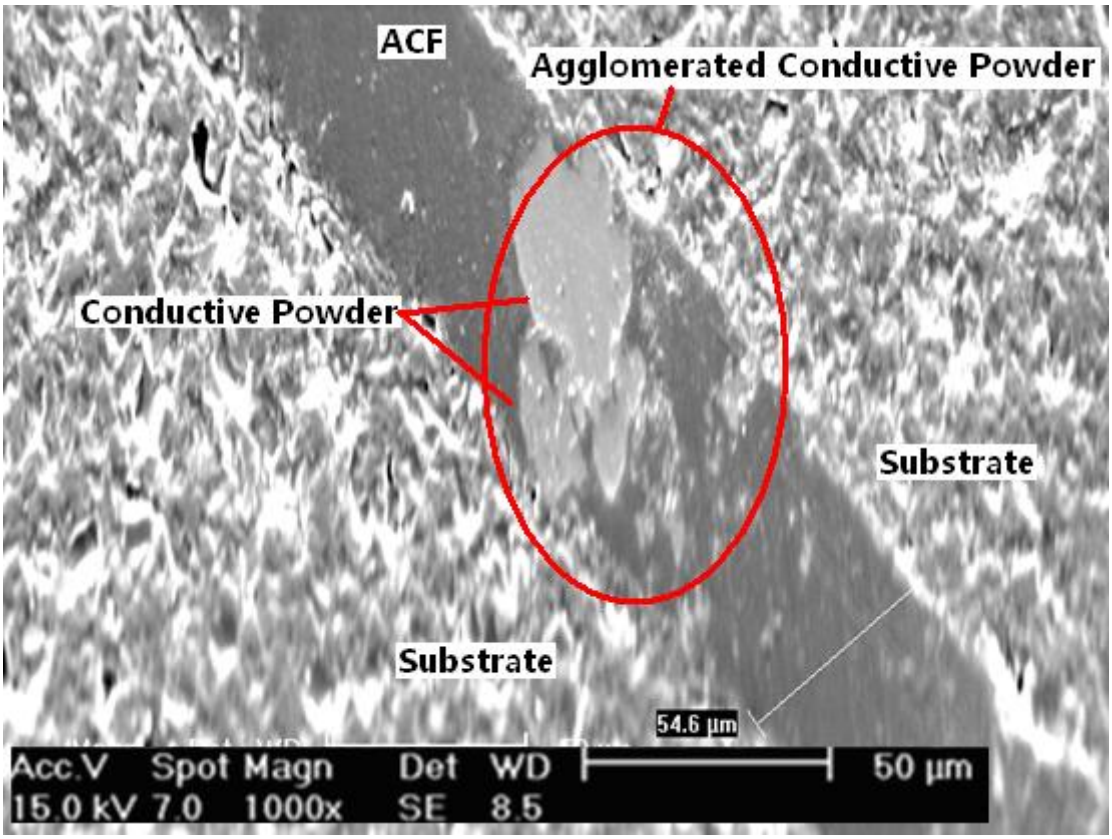

Figure 33: The cross-section of ACF joints bonded under 1.5MPa, the agglomerated conductive powder is labeled.

When the pressure applied on the samples is further increased, the agglomerated conductive powders will not be able to maintain the agglomerated state. They will crush into separate particles as shown in Figure 34. This is why the electrical resistance increases with pressure. Afterwards, gradually more agglomerated particles in the ACF will be crushed into separated particles with further increase of the pressure.

In Figure 30, when the pressure is in the region of 2.5 MPa to 6 MPa, the curve of the electrical resistance is a plateau. Although， in this region, the large agglomerated particles are broken and the effective connect area is reduced. This enables the ACF thickness to decrease with pressure. There are more and more small agglomerated particles or large single particles connecting to the electrodes, these connected particles compensate the loss of effective contact area resulting from the break-up of

the large agglomerated particles. Therefore, the resistance plateau of the ACF is formed at the pressure region from 2.5 MPa to 6 MPa.

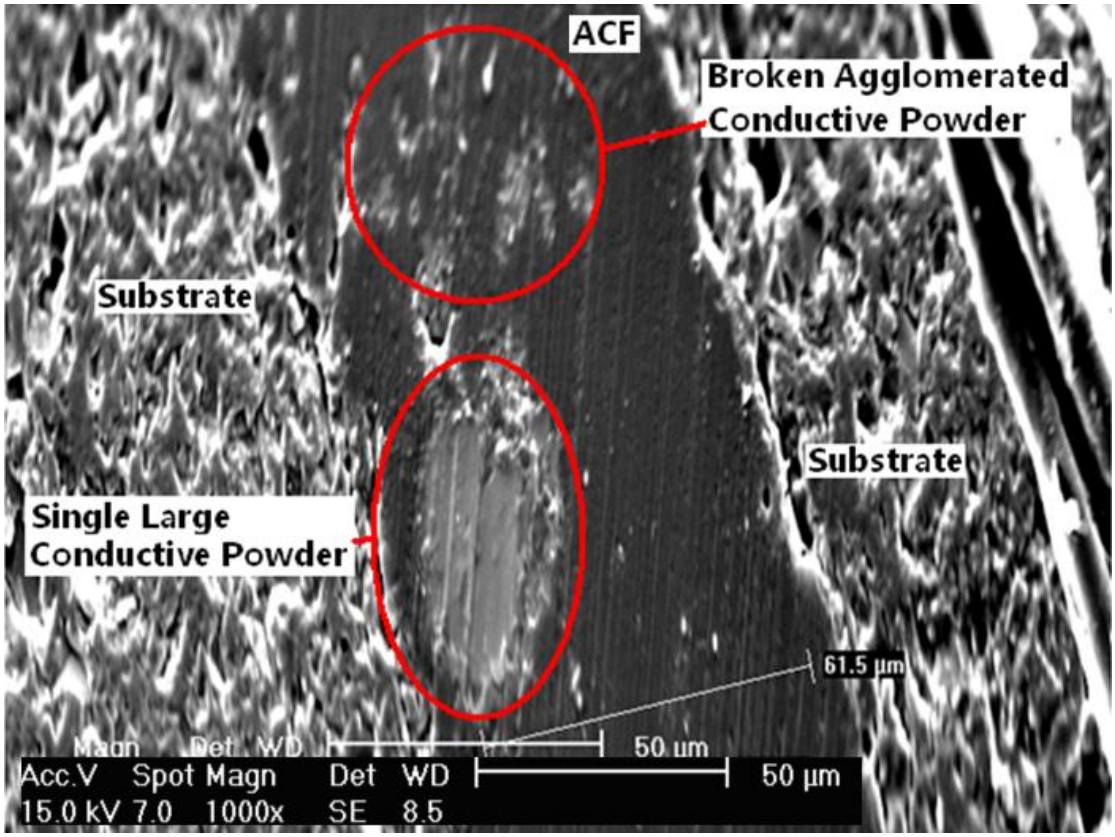

Figure 34: Cross-section of ACF joints bonded under 4.5MPa, the broken agglomerated conductive powder is labeled.

Following the first plateau in Figure 30, with further pressure increase, the electrical resistances of the samples increase to a higher value as shown in Figure 30. The results are depicted as follows: at this region, nearly all the agglomerated powders are broken and the single conductive powders play the main role in connection. The conductive particles will be deformed plastically at higher pressure with some particles cracking, which cause the loss in connection. Hence the resistance of the ACF is increased and this phenomenon is shown in Figure 35 and 36.

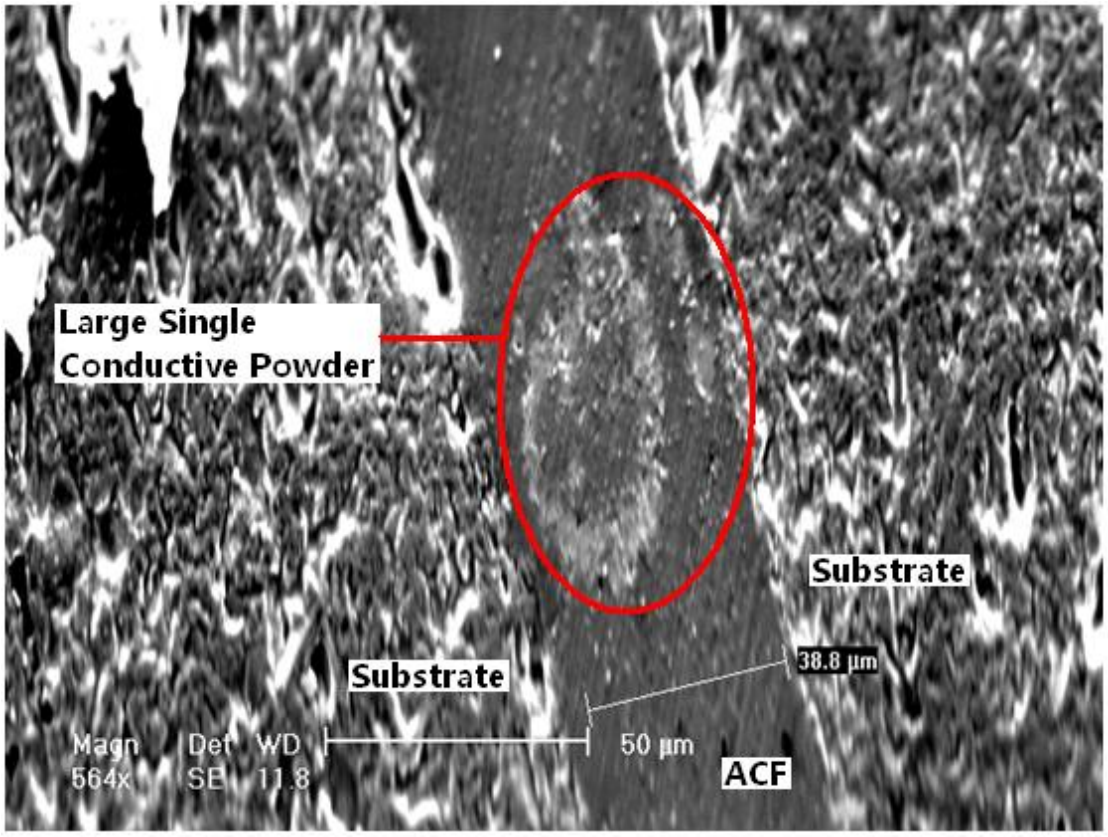

Figure 35: Cross-section of ACF joints bonded under 6MPa, the large single conductive powder is labeled.

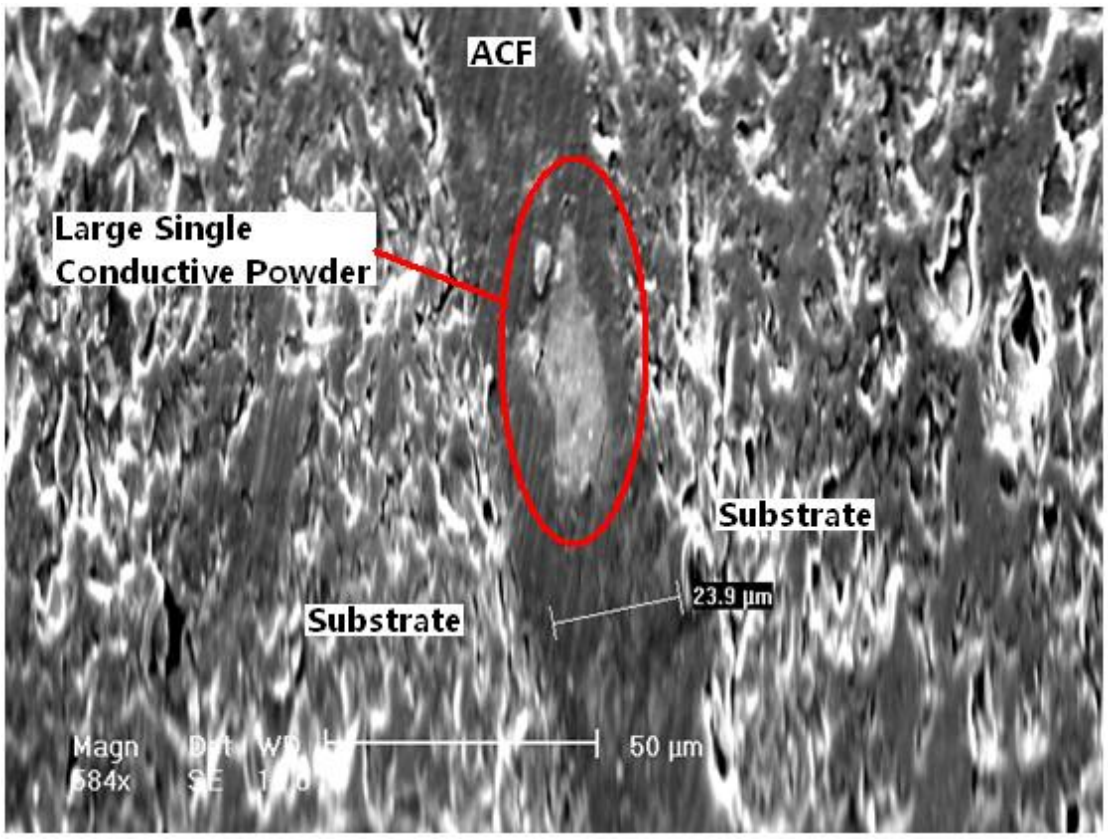

Figure 36: Cross-section of ACF joints bonded under 7.5MPa, the large single conductive powder is labeled.

The pressed area of sample is $4 \times 5 = 20$ cm^2, and according to:

$$R = \frac{\rho \cdot l}{S} \qquad \text{(Equation 6)}$$

Where R is the electrical resistance of ACF and the data are shown in Figure 30, l is length of conductive material; S is cross section area of material, ρ is electrical resistivity. In an ACF, l is equal to the thickness of the ACF and can be measured by scanning electronic microscopy (SEM); S is the contact area. Here,

l = thickness of ACF

S = contact area (1×1 cm^2)

So, from the Equation 6, data in Figure 30 and the results from SEM imaging, the relationship between electrical resistivity and pressure can be calculated and is shown in Figure 37.

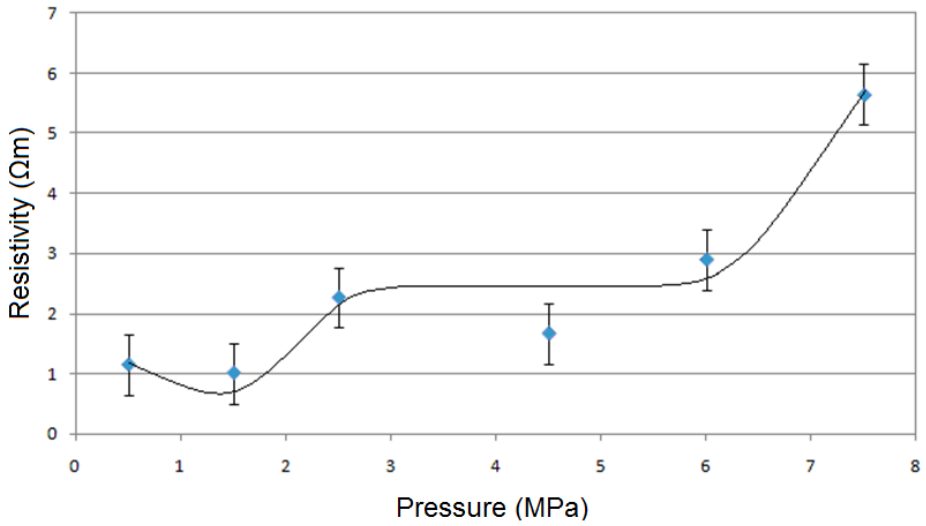

Figure 37: The dependence of Electrical resistivity of ACFs with applied pressure during curing, the data points are calculated from the result of Figure 30 and SEM.

Figure 37 presents that the electrical resistivity of the ACF various with applied pressure during curing. The data points are calculated from the result of Figure 30 and SEM. From Figure 37, the minimum electrical resistivity is $\rho = 1.00(\pm 0.5)\Omega m$

The variation of resistivity with pressure follows the same trend as the resistance, with the minimum resistivity of $\rho = 1.00(\pm 0.5)\Omega m$ at a pressure of 1.5MPa, as shown in Figure 37.

4.4. Effect of Particle Concentration on Electrical Resistance

The curve of electrical resistance against particle concentration is presented in Figure 38. The samples were bonded under the conditions of 120℃/20min/1.5MPa. As depicted in Figure 38, the electrical resistance of ACF decreases almost linearly when particle concentration increases.

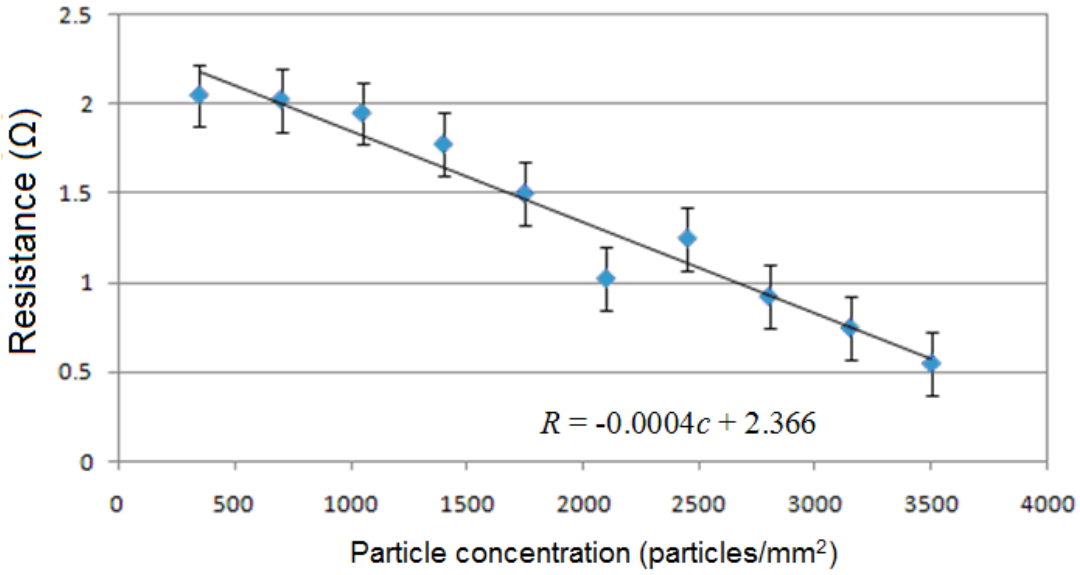

Figure 38: Electrical resistance of ACF varies as particle concentration, ACF bonded under condition of 120℃/20min/1.5MPa).

According to the data shown in Figure 38, we can obtain the following relationship equation of the electric resistance and particle concentration as follows:

$$R = -0.0004c + 2.366$$

Where c is the concentration of conductive powder.

When the bonding conditions, temperature, pressure and time, are constant and all the conductive powder is used for connection to the electrodes, the effective contact area is increased linearly as particle concentration increases such that:

$$S = a \cdot c$$

Where *S* is the effective area, and *a* is a constant.

Using: $R = \frac{\rho \cdot l}{S}$ (Equation 6)

As the bonding conditions (temperature, pressure and time) are the same and the materials of ACF are the same, therefore ρ and *l* are constant in Equation 6.

So: $R = \frac{\rho \cdot l}{ac}$,

Let $b = \frac{\rho \cdot l}{a}$ and then,

$$R = \frac{b}{c} \quad \text{(Equation 7)}$$

Therefore the electrical resistance is inversely proportional to the particle concentration in the ACF as shown in Figure 39. And the curve in Figure 38 just corresponds to the linear part of the curve as shown in Figure 39, i.e. the range of particle concentration of 350 to 3500 particles/mm^2.

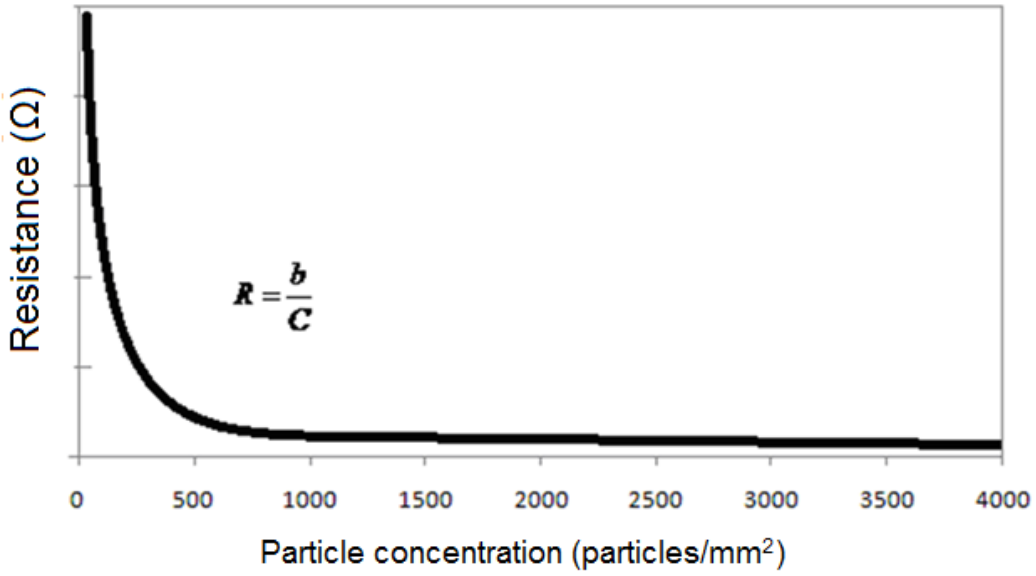

Figure 39: Relationship between electric resistance and particle density of ACF calculated from equation 7.

4.5. Effect of Service Time on Electrical Resistance

Figure 40 shows the experimental results under the following condition: samples are age treated at 80 ℃ and 80%RH and bonded at a temperature of 120 ℃, the bonding pressure was 1.5MPa and bonding time was 20 minutes; the particle concentration was 3500 particles/mm^2. The electrical resistances of the samples increase as the ageing time increases up to 350 hours. The electric resistance approached a constant stage after 350 hours.

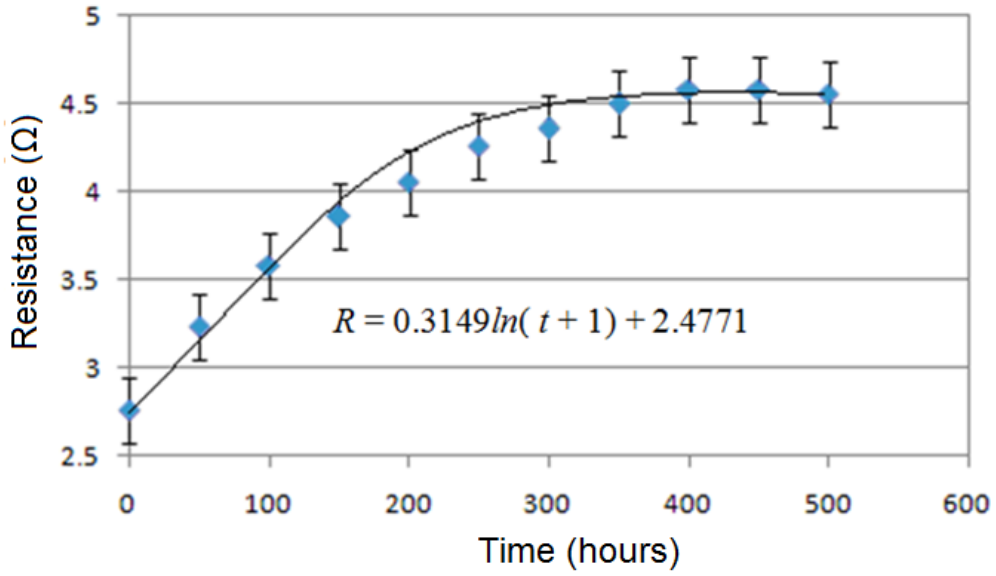

Figure 40: Electrical resistance of ACF vs. working time under condition of 80℃/80% RH. Samples were prepared under bonding conditions of 120 ℃/1.5MPa/20mins. The powder concentration was 3500 particles/mm^2.

From the curve in Figure 40, the exponential relationship between the electric resistance *R* of the ACF and the ageing time *t* can be obtained as follows:

$$R = 0.3149exp(t + 1) + 2.4771 \qquad \text{(Equation 8)}$$

According to Zhang's work (J.H. Zhang 2003), the 500 hours ageing test under condition of 80℃ and 80% RH could simulate the normal environment conditions of 5 years for ACF. The prepared ACF sample cured at 120 ℃ with 20 minutes under pressure of 1.5MPa) could therefore be expected to have a service lifetime of 5 years.

Figure 41 shows the cross section microstructure of the samples before ageing test and after ageing for 500 hours. From the microstructure, it can be seen that the thickness of the ACF has expanded by almost 30% after ageing for 500 hours, and also could be found that some defects like voids formed between the conductive particles and resin. The thickness expansion will reduce the effective contact area between the conductive particles and electrodes as shown in Figure 42. In addition,

the defects formed in the ageing process will also reduce the effective contact area between the particles. Therefore, the electrical resistance increases as service time increases.

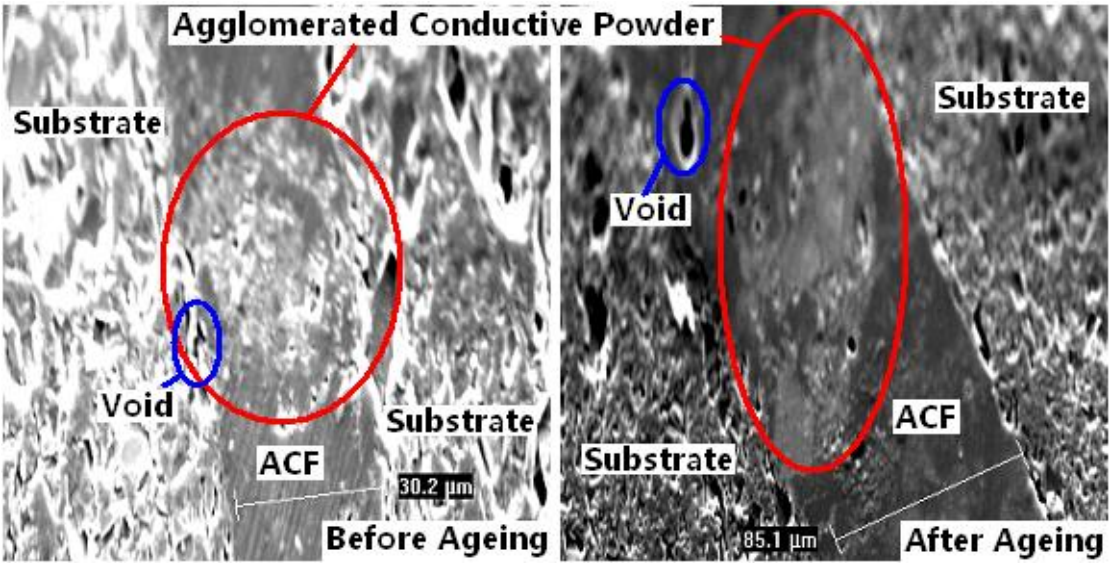

Figure 41: Cross-section of ACF joint, after 500 hours ageing test, the thickness of ACF is increased.

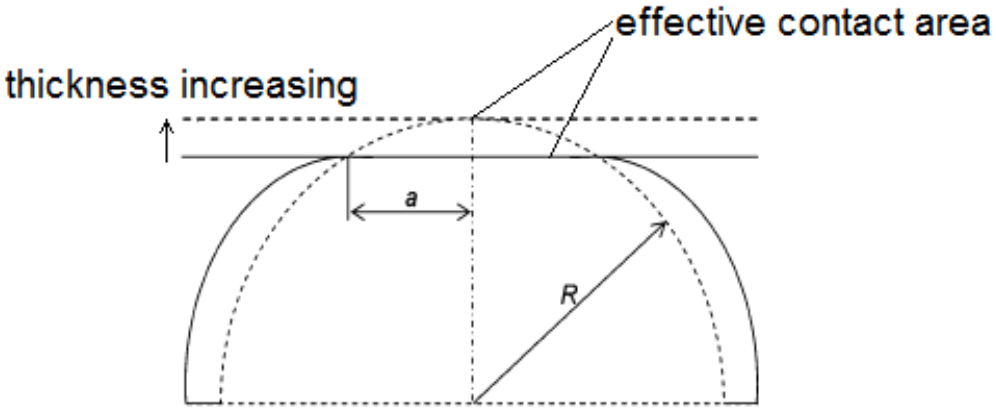

Figure 42: Schematic deformation of a half conductive particle during a long working time.

4.6. **Analysis of Defects**

Figure 43 is an optical micrograph top view of the samples. The samples with particle concentration of 3500/mm^2 were cured at 120℃ for 20 minutes under a pressure of 1.5MPa. From the pictures, agglomerated powders are easily found in the whole sample, and also the large single particles can be found in the film, the average size of the agglomerated particles is about 25μm in diameter, which is larger than the space distance of the electrodes (20μm as in photos). The large agglomerated particle and large single particles will become a bridge of two neighboring electrodes when they are located between the two electrodes as denoted in Figure 43. The large size agglomerated particles appearance in ACF might be caused by not enough mixture time; and the large single particles come from the raw materials. These two kinds of defects must be avoided during the preparation of the ACF.

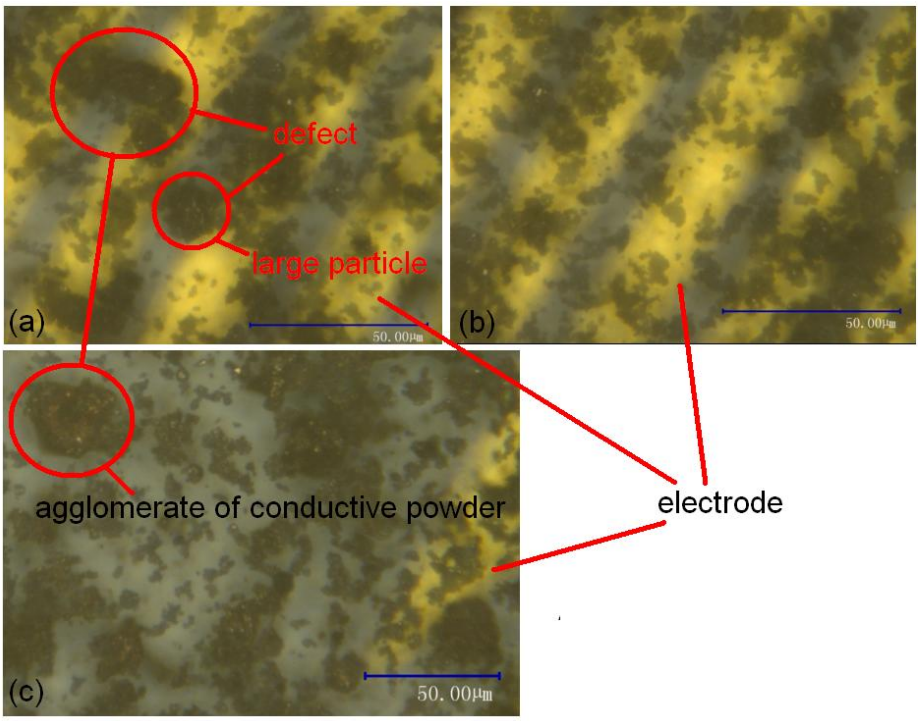

Figure 43; The morphology of conductive powders in ACF joints, where (a) is the area with defect, (b) is the area with no defect, (c) shows the agglomerate of conductive powder.

5. Conclusions

In this thesis, ACFs with different contents of conductive powders were prepared at different curing temperatures, times and different applied pressures. The properties of the ACFs have been tested and the microstructures were also analyzed. The results can be summarized as follows

1. The ACFs were synthesized from EPOFIX resin and silver coated copper conductive powders. The average minimum electric resistivity of $\rho = 1.00(\pm 0.5)\Omega m$ is achieved, when the mass ratio of EPOFIX and silver coated conductive powders is 81:19 and the curing condition is 120℃/20min/1.5MPa. The estimated service life of the prepared sample is more than 5 years.

2. There are four main factors affecting the properties of the ACF: curing temperature, curing time, applied pressure and particle concentration. The curing temperature is the most important parameter to accelerate the curing process of the ACF, but over heating of the ACF above 180℃will induce bubbles in the ACF, because the bubbles have not enough time to escape from the ACF before they are fully cured. The higher the curing temperature, the shorter the curing time.

3. The electrical resistance of the ACF varied with the applied pressure during the curing process. There are three stages: the first stage is a resistance decrease when the applied pressure is low, this stage corresponds with the contact improvement between the electrodes and the conductive particles in the ACF. The second stage is the wide range resistance plateau stage when the pressure changes from 2.5MPa to 6MPa. This stage corresponds with the agglomerated particles being crushed and more single particle connects in the ACF. The third stage is the plastic deformation of the conductive particles which results in the electrical resistance increase in the ACF.

4. The electrical resistance decreases as the particle concentration increases almost linearly when the concentration of conductive particle is larger than $350/mm^2$.

6. Future Work

In this study, because of the limitation of experiment equipment and time, the conductive particles in the prepared ACF were agglomerated together, so it is difficult to study the effect of particle size on the properties of the ACF. Future work should include the following:

1. The method of uniform dispersion of conductive particles in the epoxy resin.
2. The effect of conductive particle size distribution on the electric properties of the ACF.
3. The effect of parameters (e.g. the conductive particles concentration and size distribution, bonding pressure) on the anisotropic properties of the ACF.

7. References

Anne Lyse Bernassau (2010) **Micro-Engineering for High Frequency Ultrasound Arrays,** thesis, University of Dundee, Institute for Medical Science and Technology, May 2010

Hossack, J. A. and G. Hayward (1990). **Assessment of different pillar geometries for 1-3 composite transducers using finite element analysis**. Ultrasonics Symposium, 1990. Proceedings., IEEE 1990. IEEE, 1990: 389 – 392.

J.H. Zhang, Y.C. Chan, M.O. Alam, S. Fu (2003) **Contact resistance and adhesion performance of ACF interconnections to aluminum metallization,** Microelectronics Reliability 43 (2003) 1303–1310.

Jong-Woong Kim, Seung-Boo Jung, (2007) **Effect of bonding force on the reliability of the flip chip packages employing anisotropic conductive film with reflow process,** Materials Science and Engineering A 452–453 (2007) 267–272.

Jong-Woong Kim, Won-Chul Moon, Seung-Boo Jung, (2006) **Effects of bonding pressure on the thermo-mechanical reliability of ACF interconnection**, Microelectronic Engineering 83 (2006) 2335–2340.

M.A. Uddin, M.O. Alam, Y.C. Chan, H.P. Chan, (2004) **Adhesion strength and contact resistance of flip chip on flex packages—effect of curing degree of anisotropic conductive film,** Microelectronics Reliability 44 (2004) 505–514.

Maeda et al (1997) **Electrical connectors using anisotropic conductive film,** United States, Patent Application Publication, Pub. No.: 5624268, Pub. Date 29/04/1997.

Michael J. Adamson (1980) **Thermal expansion and swelling of cured epoxy resin used in graphite/epoxy composite materials.** Volume 15, Number 7 (1980), 1736-1745, DOI: 10.1007/BF00550593.

M.J. Rizvi, C. Bailey, H. Lu, (2008) **Failure mechanisms of ACF joints under isothermal ageing**, Microelectronics Journal 39 (2008) 1101–1107.

Myung-Jin Yim and Kyung-Wook Paik, (1999) **The Contact Resistance and Reliability of Anisotropically Conductive Film (ACF),** IEEE TRANSACTIONS ON ADVANCED PACKAGING, VOL. 22, NO. 2, MAY 1999.

Myung-Jin Yim and Kyung-Wook Paik, (1997) **Design and Understanding of Anisotropic Conductive Films (ACFs) for LCD Packaging,** IEEE (1997) 233-242.

Myung Jin Yim, Woonseong Kwon, Kyung Wook Paik (2006) **Effect of filler content on the dielectric properties of anisotropic conductive adhesives materials for high-frequency flip–chip interconnection,** Materials Science and Engineering B 126 (2006) 59–65.

Myung Jin Yim, Jinsang Hwang, Kyung Wook Paik, (2007) **Anisotropic conductive films (ACFs) for ultra-fine pitch Chip-On-Glass (COG) applications,** International Journal of Adhesion & Adhesives 27 (2007) 77–84.

Shyh-Ming Chang, Jwo-Huei Jou, Adam Hsich et al. (2001) **Characteristic study of anisotropic-conductive film for chip-on-film packaging**, Microelectronics Reliability 41 (2001) 2001-2009.

Smith, W. A. and B. A. Auld (1991). **"Modeling 1-3 composite piezoelectrics: thickness-mode oscillations." Ultrasonics, Ferroelectrics and Frequency Control**, IEEE Transactions on 38(1): 40-47.

Smith, W. A., A. Shaulov, et al. (1985). **Tailoring the Properties of Composite Piezoelectric Materials for Medical Ultrasonic Transducers.** IEEE 1985 Ultrasonics Symposium. 1985, 2: 642 – 647.

Terasaka et al (1998) **Anisotropic conductive film,** United States, Patent Application Publication, Pub. No.: 5770305, Pub. Date 23/06/2010,

Woon-Seong Kwon a, Suk-Jin Ham, Kyung-Wook Paik **(2006) Deformation mechanism and its effect on electrical conductivity of ACF flip chip package under thermal cycling condition: An experimental study** Microelectronics Reliability 46 (2006) 589–599.

Woon-Seong Kwon, Kyung-Wook Paik, (2004) **Fundamental understanding of ACF conduction establishment with emphasis on the thermal and mechanical analysis,** International Journal of Adhesion & Adhesives 24 (2004) 135–142.

Yamamoto et al (2010) **Anisotropic conductive film,** United States, Patent Application Publication, Pub. No.: US 2010/0327232 A1, Pub. D